JOURNAL OF GEOPHYSICAL RESEARCH, VOL. 104, NO. D6, PAGES 6039–6066, MARCH 27, 1999

A detailed evaluation of the stratospheric heat budget 2. Global radiation balance and diabatic circulations

Martin G. Mlynczak,[1] Christopher J. Mertens,[2] Rolando R. Garcia,[3] and Robert W. Portmann[4]

Abstract. We present a detailed evaluation of radiative heating, radiative cooling, net heating, global radiation balance, radiative relaxation times, and diabatic circulations in the stratosphere using temperature and minor constituent data provided by instruments on the Upper Atmosphere Research Satellite (UARS) between 1991 and 1993 and by the limb infrared monitor of the stratosphere (LIMS) instrument which operated on the Nimbus-7 spacecraft in 1978-1979. Included in the calculations are heating due to absorption of solar radiation from ultraviolet through near-infrared wavelengths and radiative cooling due to emission by carbon dioxide, water vapor, and ozone from 0 to 3000 cm^{-1} (∞ - 3.3 μm). Infrared radiative effects of Pinatubo aerosols are also considered in some detail. In general, we find the stratosphere to be in a state of global mean radiative equilibrium on monthly timescales to within the uncertainty of the satellite-provided measurements. Radiative relaxation times are found to be larger in the lower stratosphere during UARS than LIMS because of the presence of Pinatubo aerosols. The meridional circulations in the upper stratosphere as diagnosed from the calculated fields of net heating are generally stronger in the UARS period than during the LIMS period, while the lower stratosphere meridional circulations are stronger during the LIMS period. A climatology of these calculations is available to the community via a World Wide Web interface described herein.

1. Introduction

In this paper we present results of an in-depth investigation of the stratospheric heat budget and radiative balance as diagnosed from stratospheric composition measurements provided by orbiting satellite experiments. Specifically, we compute monthly averaged radiative heating, infrared cooling, net radiative heating, diabatic circulations, and radiative relaxation times in the stratosphere. We utilize the data sets of stratospheric temperature and minor species concentration (e.g., O_3, H_2O, NO_2) provided by the limb infrared monitor of the stratosphere (LIMS) experiment in 1978-1979 [*Gille and Russell*, 1984] and by the numerous instruments on the Upper Atmosphere Research Satellite (UARS) [*Reber et al.*, 1993] from 1991 to 1993. A total of 18 months of data are analyzed, 5 months of LIMS data and 13 months of UARS data. Our objective is to diagnose the radiative properties of the stratosphere using only data derived from satellite observations. This approach will provide a key test of the ability to derive radiative and dynamical properties of the atmosphere from satellite observations alone.

There have been numerous studies of the stratospheric heat budget and associated circulations dating back 40 years. The driving force behind many of these studies was the need to understand the distribution and variability of stratospheric ozone in order to assess possible anthropogenic effects on the ozone layer. The studies tend to fall into two categories: studies of the heat budget with assessments of departures from radiative equilibrium and studies of the meridional diabatic and residual circulations. Some studies are observation based (e.g., use satellite-derived fields of temperature and computed fields of heating and cooling), while others are more theoretical in nature. It is not possible for us to review here this broad body of work. We therefore review those papers important for their historical context or which are similar in scope to ours, namely, studies using satellite data to diagnose the stratospheric heat budget and diabatic circulations. The purpose is to place our results in the context of previous studies.

[1]NASA Langley Research Center, Hampton, Virginia.
[2]G & A Technical Software, Newport News, Virginia.
[3]National Center for Atmospheric Research, Boulder, Colorado.
[4]NOAA Aeronomy Laboratory, Boulder, Colorado.

Paper number 1998JD200099.
0148-0227/99/1998JD200099$09.00

The original study of the heat budget of the middle atmosphere is that of *Murgatroyd and Goody* [1958, hereinafter referred to as MG] covering the altitudes of 30 km to 90 km. MG computed zonal mean solar heating rates due to absorption of ultraviolet radiation by ozone and molecular oxygen and infrared cooling due to emission by carbon dioxide at 15 μm. Radiative effects involving water vapor and dust were acknowledged but not included. MG found radiative heating and cooling to balance to within 2 K/d at low to midlatitudes and significant departures from local radiative equilibrium at the poles characterized by an excess of heating over cooling in the summer pole and excess of cooling over heating at the winter pole.

The work of MG was followed by that of *Murgatroyd and Singleton* [1961, hereinafter refered to as MS] who attempted to estimate the meridional circulation of the stratosphere using the heating rates of MG. MS neglected horizontal heat transport by horizontal eddies, which allowed calculation of the mean meridional circulation from a specification of the heating rate and temperature structure. The circulations calculated by MS were qualitatively in agreement with observed features; for example, the predicted subsidence in the polar night mesosphere is consistent with the observed warm winter mesosphere temperatures, and similarly, the predicted upwelling in the cold summer mesosphere is consistent with the observed cold temperatures there. However, MS were unable to justify the neglect of meridional eddy heat fluxes, and thus questions remained as to whether their derived circulation was representative of actual middle atmospheric transport. At the same time, efforts were made to explain the processes that maintained the warm winter mesosphere in the absence of solar illumination. *Kellog* [1961] postulated that heat release from exothermic recombination of atomic oxygen transported into the mesosphere from the thermosphere provided the heat source. *Young and Epstein* [1962] further examined Kellog's hypothesis and found that a combination of heat release by exothermic reactions and adiabatic compression could provide the required energy to warm the mesosphere.

The situation was finally clarified by *Dunkerton* [1978] who qualitatively and quantitatively drew a distinction between Eulerian-mean and Langrangian-mean circulations. Dunkerton drew upon the noninteraction theorems of *Charney and Drazin* [1961], *Boyd* [1976], and *Andrews and McIntyre* [1976] to show that when waves are steady and conservative, a Eulerian mean meridional circulation is established which identically cancels the eddy heat fluxes of the waves themselves. In fact, there is a large degree of cancellation between the eddy flux divergence and the mean advection terms even when the waves are not steady and conservative. Dunkerton pointed out that net transport is more clearly described in terms of Lagrangian mean advection [*Andrews and McIntyre*, 1976] and that the diabatic circulation (which can be derived from the Eulerian-mean net heating and temperature distribution) is a good approximation to the Lagrangian-mean motion. Thus under these assumptions the work of MS was in fact representative of middle atmospheric transport to the extent that the radiative heating and cooling and thermal structure were accurate.

Following the work of Dunkerton the review by *London* [1980] identified all of the sources and sinks of energy included in our present work. However, there was still not a consistent, global data set of temperature and constituents from which to assess the stratospheric heat budget and to derive meridional circulations for comparisons with observed species distributions. The situation changed upon publication of the LIMS data in the mid-1980s. *Kiehl and Solomon* [1986, hereinafter referred to as KS] presented the first global observation-based study of the stratospheric heat budget using LIMS data. KS found distributions of net heating and cooling similar to those of MS but different in magnitude of absolute heating and cooling. KS also pointed out that the stratosphere is expected to be in radiative equilibrium on a globally averaged basis. Thus a test of the quality of the radiative transfer algorithm, the spectral data, and the observations can be achieved by computing the global mean radiative balance. For the month of January 1979, KS showed that the computed global mean solar heating and infrared cooling balanced to within about 25% below 42 km and to about 10% between 42 and 52 km. These differences correspond to approximately 0.5 K/d to 1.0 K/d depending on altitude. As we will show below, we have made significant progress in the capability to calculate global mean net stratospheric heating. We find that the computed global mean solar heating and infrared cooling agree to within 12% using the LIMS data set and within 10% using the UARS data set at most altitudes within the stratosphere. These percentages correspond to differences in the range of 0.03 K/d to 1.0 K/d.

The work of KS was followed immediately by a paper by *Solomon et al.* [1986a] in which the LIMS data and computed fields of radiative heating and cooling of KS were used to calculate, for the first time, the global diabatic circulation from observations. As with the radiative computations of KS, the circulations presented by *Solomon et al.* [1986a] were in general agreement with those of MS but with significant differences in the actual details of the diagnosed circulations. For example, the meridional circulations calculated by Solomon et al. are much more vigorous than those of MS, and there is a large meridional gradient in the vertical wind field near the tropical stratopause in January and February which was not evident in the MS calculations. Solomon et al. attributed this feature to the semiannual oscillation.

Shortly after the work by KS and Solomon et al., papers by *Gille and Lyjak* [1986, 1987] also reported studies of the stratospheric heat budget and circulations using LIMS data. These studies differed from earlier LIMS work primarily in the radiation algorithms

used, in the inclusion of minor heat sources (such as near-infrared absorption by CO_2, H_2O, and O_2), and in the attempt to include tropospheric and cloud effects. An examination of the monthly net heating, calculated by the two groups for the seven LIMS months, shows results for heating, cooling, and net heating which are broadly consistent in terms of regions of net heating and cooling but with important differences in the magnitudes, especially of the net heating and the computed diabatic circulations. This fact was pointed out in the study (again using LIMS data but set in isentropic coordinates) by *Pawson and Harwood* [1989] who also commented on the need for a consistent adjustment of the net heating rates to achieve global mean radiative equilibrium prior to computing the diabatic circulations.

More recently, stratospheric diabatic and residual circulations have been computed using data from the Microwave Limb Sounder (MLS) instrument on the Upper Atmosphere Research Satellite (UARS) [*Eluszkiewicz et al.*, 1996, hereinafter referred to as E1] and from the cryogenic limb array etalon spectrometer (CLAES) instrument also on the UARS [*Eluszkiewicz et al.*, 1997, hereinafter referred to as E2]. These studies are similar to ours with the following exceptions: First, the papers of Eluszkiewicz et al. focus primarily on the diagnosed circulations and not on the global energy balance of the stratosphere. The work herein focuses on both topics. Second, in our work the radiative effects of Pinatubo aerosols are routinely included in the heat balance computations and in the calculations of the diabatic circulations. Third, we compute circulations for monthly averages, while the work reported by E1 and E2 generally uses quasi-2-week averages. Because our work makes use of the MLS temperatures, water vapor, and ozone for the UARS period, we compare our results with those presented by E1. As will be shown below, there is similarity in the computed meridional circulations, but important differences in magnitude do exist between the two sets of calculations.

The purpose of our work is to use LIMS and UARS satellite observations of temperature and minor species in concert with accurate radiative transfer codes to evaluate (1) the rates of heating and cooling in the stratosphere, (2) the net heating in the stratosphere, (3) the global energy balance in the stratosphere, (4) the monthly diabatic circulation, (5) the radiative effects of Pinatubo aerosols on the heat budget, (6) the radiative relaxation time of the stratosphere, and (7) differences between the 1970s (LIMS) and the 1990s (UARS). A key feature of our studies is the use of accurate and validated radiative transfer codes LINEPAK and BANDPAK [*Gordley et al.*, 1994; *Marshall et al.*, 1994], which in some instances have been used to generate the satellite data sets. The radiative transfer calculation approaches, used to generate the results presented in this paper are given in our previous paper [*Mertens et al.*, this issue (hereinafter referred to as part 1)]. Our goal is to conduct a consistent set of radiative transfer calculations for evaluating stratospheric radiative properties on the only extant satellite data sets. A total of 18 months of data from LIMS and UARS have been analyzed. We find the stratosphere to be in a state of global mean radiative equilibrium on a monthly scale to within the uncertainties of the measurements and the computation approaches, and without having to do large adjustments to achieve global mass balance. We do find differences in the diagnosed circulations from the LIMS and UARS data which probably reflect natural variability of the stratosphere. We have also prepared a climatology of our diabatic heating calculations and circulations which is made available to the community via the World Wide Web.

The radiative transfer codes and algorithms are presented in part 1 which immediately precedes this paper. In this present paper we give a description of the input satellite data, and its preparation in section 2, followed by results in section 3. A summary, including details on accessing the 18 month climatology, is given in section 4.

2. Input Data

The stratospheric radiative properties and circulations are computed and compared for two periods: November 1978 through May 1979, using data from the limb infrared monitor of the stratosphere (LIMS) instrument on the Nimbus-7 spacecraft [*Gille et al.*, 1984], and October 1991 through April 1993, using level 3AL and 3AT data from various instruments aboard the Upper Atmosphere Research Satellite (UARS) [*Reber et al.*, 1993]. UARS temperature, water vapor, and ozone data are taken from the Microwave Limb Sounder (MLS) [*Barath et al.*, 1993]. UARS nitrogen dioxide data are taken from the cryogenic limb array etalon spectrometer (CLAES) [*Roche et al.*, 1993] and from the improved stratospheric and mesospheric sounder (ISAMS) [*Taylor et al.*, 1993]. Three months prior to the launch of UARS, Mount Pinatubo in the Philippines erupted and injected an enormous volume of aerosol into the lower stratosphere, which was transported across the globe in a matter of months. The volcanic aerosols, which added significant opacity in the lower stratosphere, are included in the infrared cooling rate calculations during the UARS period. Aerosol extinction data are taken from the Halogen Occultation Experiment (HALOE) [*Russell et al.*, 1993].

The UARS orbit has a 57° inclination with respect to the equatorial plane, restricting the latitudinal coverage at any one time to about 80° in one hemisphere and 34° in the other hemisphere [*Reber et al.*, 1993]. Approximately every 36 days the spacecraft is rotated in a yaw maneuver by 180° in its orbital track, reversing the latitudinal coverage between the hemispheres. Therefore "monthly" zonal mean temperature and trace gas concentrations are computed by averaging the fields over a period roughly 15 days prior to and subsequent to a yaw

maneuver and in 4° latitude bins from 80° N to 80° S. Thirteen "months" are defined in Table 1, hereinafter called yaw periods, corresponding to the first 17 months of UARS operation, in which we calculate the radiative properties of the stratosphere. These months exclude the May-June 1992 period when the UARS satellite was powered off due to a solar array drive problem, and the period beyond April 23, 1993, when the MLS H_2O radiometer stopped working. CLAES also ceased to operate in May 1993. Again, it is our objective to use only data derived from satellite observations in the calculations. The UARS level 3AL and 3AT data were obtained from the NASA Goddard Space Flight Center Distributed Access Archive Center (DAAC).

The UARS profiles at each latitude and for each yaw period are tabulated at the standard UARS pressure levels,

$$p(i) = 1000.0 \times 10^{(-i/6)}, \quad (1)$$

where pressure is in units of hPa (mbar). Infrared cooling rates are calculated at pressure levels between 1000 hPa and 0.046 hPa ($i = 0, 1, \ldots, 26$). Solar heating rates were calculated at pressure levels from 100 hPa to 0.1 hPa ($i = 6, 7, \ldots, 24$). The vertical range useful for scientific studies, however, is restricted to a subset of the above pressure levels, depending on the specific parameter and determined from the data validation analysis. The useful vertical ranges for each UARS input parameter used in this study are given in Table 2 and discussed in more detail below.

The Nimbus-7 spacecraft was placed in a nearly circular, Sun-synchronous orbit, with LIMS viewing at 146.5° clockwise from the velocity vector [*Gille et al.*, 1984]. The orbital and viewing geometries combine to give a latitudinal coverage that extends from 84° N to 64° S. The LIMS temperature and trace gas concentrations are obtained from the LIMS map archival tape (LAMAT) archive product [*Remsberg et al.*, 1990]. Data on the LAMAT archive are tabulated on pressure surfaces from 100 hPa to 0.05 hPa. Similar to UARS data, the useful vertical range for scientific studies covers a subset of the above pressure levels. Table 3 lists the vertical ranges for the LIMS parameters. Other data sources, where available, were coupled to the LIMS data set to extend the latitudinal coverage from 88° N to 88° S and to extend the vertical coverage to 1000 hPa and to 0.05 hPa, as described in the sections below. Monthly zonal mean temperature and trace gas concentrations were computed in 4° latitude bins and over the same 30 day periods as the UARS data. However, the LIMS mission lasted only 6 months. Consequently, data are only available from YAW2-YAW6 (November-December 1978 to April-May 1979, see Table 1). Finally, the profiles are linearly interpolated in log pressure from the LAMAT pressure levels to the standard UARS pressure levels given in (1). This pro-

Table 1. Monthly Averaging Periods and CO_2 Concentrations

Month	Averaging Period	Year	CO_2, ppmv
YAW1	10/19 to 11/18	UARS, 1991	UARS, 346.18
		LIMS, N/A	LIMS, N/A
YAW2	11/19 to 12/19	UARS, 1991	UARS, 346.30
		LIMS, 1978	LIMS, 327.00
YAW3	12/30 to 1/29	UARS, 1991-1992	UARS, 346.43
		LIMS, 1978-1979	LIMS, 327.00
YAW4	1/30 to 2/29	UARS, 1992	UARS, 346.56
		LIMS, 1979	LIMS, 327.00
YAW5	3/8 to 4/7	UARS, 1992	UARS, 346.75
		LIMS, 1979	LIMS, 327.00
YAW6	4/16 to 5/16	UARS, 1992	UARS, 346.93
		LIMS, 1979	LIMS, 327.00
YAW7	7/29 to 8/28	UARS, 1992	UARS, 347.35
		LIMS, N/A	LIMS, N/A
YAW8	9/6 to 10/6	UARS, 1992	UARS, 347.50
		LIMS, N/A	LIMS, N/A
YAW9	10/14 to 11/13	UARS, 1992	UARS, 347.68
		LIMS, N/A	LIMS, N/A
YAW10	11/14 to 12/14	UARS, 1992	UARS, 347.81
		LIMS, N/A	LIMS, N/A
YAW11	12/25 to 1/24	UARS, 1992-1993	UARS, 347.93
		LIMS, N/A	LIMS, N/A
YAW12	1/25 to 2/24	UARS, 1993	UARS, 348.06
		LIMS, N/A	LIMS, N/A
YAW13	3/4 to 4/3	UARS, 1993	UARS, 348.20
		LIMS, N/A	LIMS, N/A

Table 2. Useful Pressure Range of UARS Parameters

Parameter	Pressure, hPa
MLS T	22-0.46
MLS O_3	46-0.46
MLS H_2O	46-0.22
CLAES NO_2[a]	20-2
HALOE 5.26 μm AEREXT	100-10

[a]No reported range for ISAMS NO_2.

cessing step was performed to remove anomalous spikes in the infrared cooling rates near 16 hPa, caused by a discontinuous change in level spacing on the LAMAT archive.

Zonal mean diabatic heating and circulations are computed over the yaw periods listed in Table 1. Zonal mean diabatic heating rates are in principle obtained by calculating the solar heating and infrared cooling rates for each measurement profile and then averaging around latitude circles. However, for computational efficiency, we first calculate zonal averages of the input temperature and minor constituent data and then compute diabatic heating and circulations. The impact of this approximation is assessed in section 3.1. In general, the heating rate error introduced by first zonally averaging the input data is of the order of 0.05 K/d, which is comparable to the small error introduced by the computational scheme and well below the error introduced by uncertainties in the satellite data itself. Thus the error introduced by using zonally averaged input fields contributes only a small fraction to the calculated global radiative imbalance.

Infrared cooling rates are calculated from monthly zonal daytime plus nighttime averages of temperature, water vapor, and ozone. During the UARS period, monthly zonal mean aerosol extinctions at 5.26 μm are also computed for use in assessing radiative heating and cooling by the Pinatubo aerosol layer, as discussed below. Carbon dioxide is assumed to be uniformly mixed and the abundances for each yaw period are given in Table 1. An example of the LIMS and UARS data is given in Figure 1 which shows zonally averaged temperature, ozone, water vapor, nitrogen dioxide, and aerosol extinction at equinox (YAW 5). The construction of these

Table 3. Useful Pressure Range of LIMS Parameters

Parameter	Pressure, hPa
T	100-1.0
O_3	100-0.1
H_2O	100-1.0
NO_2	30-3.0

monthly zonal mean fields for each input parameter is discussed below. Note that for the LIMS period we are assuming that stratospheric aerosol concentrations are negligible.

2.1. Temperature

UARS monthly zonal mean temperature profiles are calculated from MLS level 3AL version 3 data. The useful vertical range reported in the validation paper [*Fishbein et al.*, 1996] is from 22 hPa to 0.46 hPa. Above 0.22 hPa the profiles are based on a climatology developed by the UARS science team. Below 46 hPa the profiles are linearly interpolated from the National Meteorological Center (NMC) daily analysis, or climatology if necessary.

Because of the UARS orbital track, it is not possible for certain yaw periods to have daytime profiles at all latitudes from 80°N to 80°S. The profiles of the latitude bins poleward of the bin containing the last available profile were taken to be equal to that profile. For MLS temperatures, the last available latitude bins are 76° N for YAW1, 64° N for YAW2 and YAW3, 76° S for YAW6, and 64° S for YAW10 and YAW11.

LIMS monthly zonal mean temperature profiles are calculated from the LAMAT archive product. LAMAT temperature coverage is from 100 hPa to 0.1 hPa and from 84° N to 64° S. The vertical range useful for scientific studies is from 100 hPa to 1.0 hPa [*Gille et al.*, 1984]. The latitudinal coverage is extended poleward of 64°S, and the vertical range was extended to 0.05 hPa using NMC data. Daily NMC temperatures are averaged over the LIMS yaw periods and linearly interpolated in latitude and pressure. The profiles at 84°N are extended to 88°N. Tropospheric temperatures were taken from the climatology included in the MLS 3AL data file. Finally, the temperature profiles are linearly interpolated in log pressure to the standard UARS grid.

2.2. Ozone

Level 3AL version 3 ozone data measured from the MLS 205-GHz radiometer are used to calculate monthly zonal mean profiles. *Froidevaux et al.* [1996] reported in the MLS ozone validation paper that the useful vertical range is from 46 hPa to 0.46 hPa. Additional information on MLS ozone quality can be found in the articles by *Cunnold et al.* [1996a, b]. Outside the range of pressures above 100 hPa and below 0.46 hPa the data are mostly climatological.

For the same reason as discussed in the previous section, it is not possible for certain yaw periods to have daytime profiles at all latitudes from 80°N to 80°S. Similarly, the profiles of the latitude bins poleward of the bin containing the last available profile were taken to be equal to that profile. The last available latitudes for MLS ozone are the same as for MLS temperatures.

Monthly zonal mean ozone profiles during the LIMS period are calculated from the LAMAT archive. The

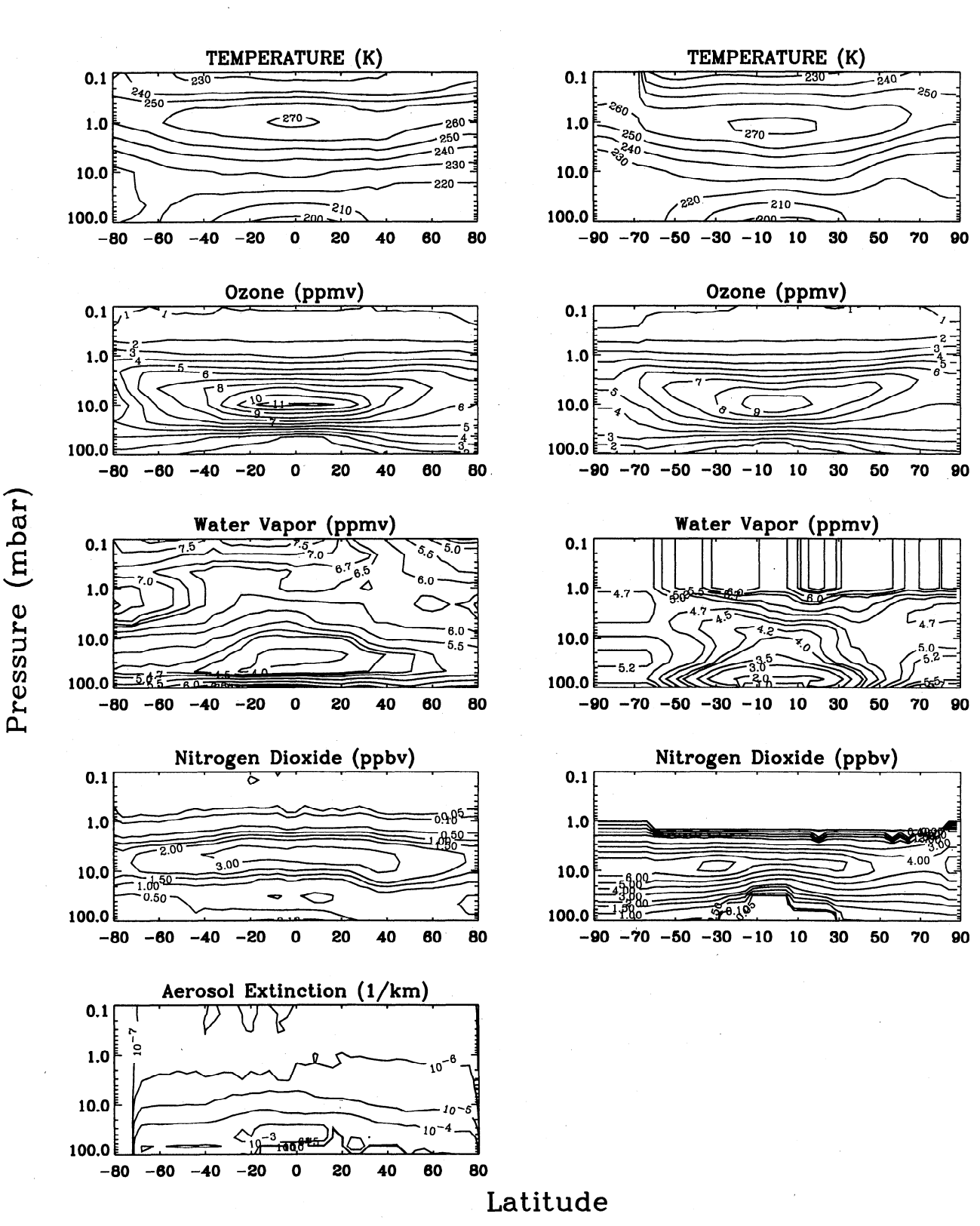

Figure 1. Sample zonal mean (day plus night) temperature data and minor constituent data for YAW5 used to calculate infrared cooling rates. Data sources are described in the text. YAW5 corresponds to equinox.

validation analysis was conducted by *Remsberg et al.* [1984]. The effects of non-LTE in the LIMS daytime ozone data [*Solomon et al.*, 1986b; *Mlynczak and Drayson*, 1990a, b] were reduced by computing the daytime ozone concentrations using the LIMS nighttime ozone concentrations multiplied by the latitude-dependent day/night ozone ratios from the Garcia-Solomon model [*Garcia et al.*, 1992; *Garcia and Solomon*, 1994]. This procedure only affects the ozone above about 50 km (1 hPa) by reducing the magnitude of the daytime ozone concentration which was artificially high due to non-LTE emission from ozone and carbon dioxide that was not accounted for in the LIMS (LTE) retrieval. LAMAT ozone coverage is from 100 hPa to 0.1 hPa and from 84°N to 64°S. The latitudinal coverage was extended from 64°S to 80°S and the vertical range was extended from 1.0 hPa to 0.05 hPa using SBUV data. The profiles at 84°S and 88°S were extended from the profiles at 80°S. Similarly, the profiles at 84°N and 88°N were extended from the profiles at 80°N. Tropospheric ozone data were taken from the climatology included in the MLS (205-GHz) level 3AL data file. Finally, the ozone profiles were linearly interpolated in log pressure to the standard UARS grid.

2.3. Water Vapor

Similar to UARS temperature and ozone, MLS level 3AL version 3 data are used to calculate monthly zonal mean water vapor profiles. The useful vertical range for MLS water vapor is from 46 hPa to 0.2 hPa, as reported in the validation paper by *Lahoz et al.* [1996]. Outside this range the data are mostly climatological.

The LAMAT product is used to calculate LIMS monthly zonal mean water vapor profiles. The useful vertical range is from 100 hPa to 1.0 hPa, as reported by *Russell et al.* [1984b]. Tropospheric water vapor data were taken from the climatology included in the MLS level 3AL data file. No other data sources were used to extend the latitude and vertical range above 1hPa. The water vapor concentrations at 1.0 hPa are extended to 0.05 hPa for each latitude bin. Similarly, the profiles at 64°S were extended to 88°S, and from 84°N to 88°N. The profiles are finally interpolated, linearly in log pressure, to the standard UARS grid.

2.4. Nitrogen Dioxide

Monthly zonal mean nitrogen dioxide profiles are calculated from both CLAES and ISAMS level 3AL data. CLAES nitrogen dioxide data are missing prior to January 10, 1991. Therefore ISAMS version 10 data are used for YAW1-YAW2 and during the first 10 days in YAW3. Afterwards CLAES version 7 data are used. The useful vertical range for CLAES nitrogen dioxide is reported to be 20 hPa to 2 hPa [*Reburn et al.*, 1996]. To our knowledge, no recommended vertical range for scientific analysis has been reported for the ISAMS nitrogen dioxide data.

Daytime averages of nitrogen dioxide suffer from the same restriction on latitude coverage described above for daytime averages of temperature and ozone. The coverage is extended in the same way: profiles of the latitude bins poleward of the bin containing the last available profile were set equal to that profile. For ISAMS and CLAES nitrogen dioxide data, the last available latitudes are typically 76°N and occasionally 64°N. Moreover, numerous data points are missing at UARS level 0.1 hPa. The nitrogen dioxide concentrations at 0.15 hPa were extended to 0.1 hPa.

The LAMAT product is used to calculate monthly zonal mean nitrogen dioxide profiles during the LIMS period. The useful vertical range is from 30 hPa to 3 hPa [*Russell et al.*, 1984a]. No other sources were used to extend vertical and latitudinal coverage. Because nitrogen dioxide is difficult to detect above 2 hPa, and is very near to zero, the concentrations above 2 hPa were set equal to zero [*Kiehl and Solomon*, 1986]. The profiles at 64°S are extended to 88°S, and from 84°N to 88°N. Finally, the profiles are linearly interpolated in log pressure to the standard UARS grid.

2.5. Aerosol Extinction

HALOE aerosol extinctions at 5.26 μm, corresponding to the gas-filter nitric oxide (NO) channel, are used to develop an infrared aerosol extinction model. The model is described in part 1. Monthly zonal mean extinction data are calculated using level 3AT version 18 data. Validation studies by *Hervig et al.* [1996] suggest that the useful vertical range is from 100 hPa to 10 hPa.

HALOE uses the method of solar occultation to measure profiles of limb-path solar attenuation by the Earth's atmosphere as the Sun rises and sets, as viewed from the spacecraft. The measurement coverage provides two longitude sweeps per day, one at the latitude of sunsets and the other at the latitude of sunrises. The progression of sunrise and sunset latitudes, due to the 57° inclination orbit of UARS, affords near-global coverage in periods of 20 to 30 days. Consequently, because of the HALOE sampling pattern, there are varying locations of the globe which are not observed during each yaw period.

3. Results

3.1. Zonal Mean Heating and Cooling

In this section we present the climatology of zonal mean heating and cooling for LIMS and UARS periods. In all computations we first zonally average the temperature and minor constituent data and then calculate the solar heating and infrared cooling rates based on the zonally averaged fields. Because of the volume of data involved we choose this approach rather than first calculating global fields of heating and cooling and then zonally averaging those fields. To test the appropriateness of this approach we analyzed a simple case

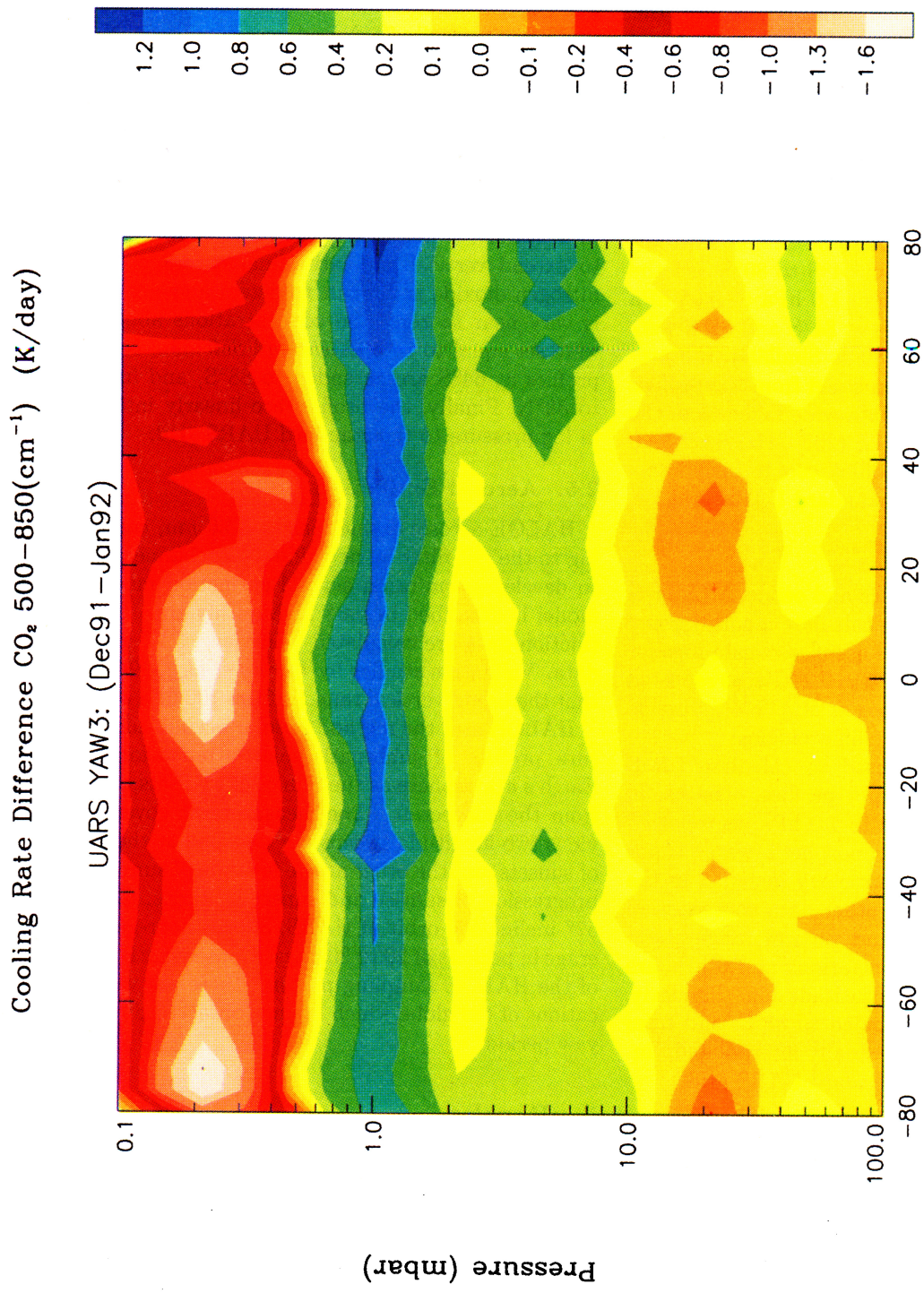

Plate 1. Latitude-pressure cross sections of zonal mean cooling rates differences (K/d) from CO_2 in the 500-850 cm^{-1} region. Cooling rate differences are defined as zonally averaged cooling rates minus cooling rates calculated from zonally averaged temperature profiles. Cooling rates were calculated using every MLS level 3AT temperature profile available from the DAAC during UARS YAW3 period (Dec91 to Jan92) (28 UARS days, 36,914 temperature profiles) before zonal averaging was done.

and considered the impact on the zonal mean cooling rates and the global-average cooling rate for the CO_2 15 μm fundamental band. We computed global fields of infrared cooling and then calculated their zonal averages and global averages for comparison with the cooling calculated using the zonally averaged temperature data. Plate 1 shows zonal mean cooling rate differences between the two approaches for UARS YAW3 (December 1991 to January 1992). The differences are generally within $\pm$0.2 K/d between 10 and 100 hPa. Over much of the globe the differences are less than 0.1 K/d between 10 and 100 hPa. The largest differences in the stratosphere occur near the temperature maximum, with differences reaching 1 K/d. There is also a region of enhanced cooling rate differences between 3 and 7 hPa at middle to high latitudes in the winter hemisphere. In the mesosphere the absolute differences exceed 0.4 K/d at altitudes above 0.5 hPa and are as high as 2 K/d in the tropical and polar summer regions. The MLS data meet the climatology around 0.5 hPa (see also Table 2). It is our belief that poor meshing of the temperature data with the climatology is causing the large errors in the lower mesosphere and not the method of zonal averaging the cooling rates. Table 4 shows the comparison of the global average cooling rates between the two approaches. As can be seen, there is very little difference between the two approaches, typically 1% to 3% at pressures less than 100 hPa and greater than 1 hPa. The largest absolute difference occurs near the stratopause. This difference is a consequence of the coarse vertical layering of UARS data in the region of rapid vertical temperature gradients which we discussed in paper 1. We would anticipate that the largest errors in our approach would be in the infrared calculations due to the sensitivity of radiative exchange to the temperature field. Because of the relatively small errors associated with our approach (which are due to layering and not to zonal averaging, per se) we conclude that it is appropriate to zonally average the temperature and constituents first and then calculate the cooling (and heating) rates for the zonally averaged profiles.

Figure 2 shows plots of total solar heating and total infrared cooling for the LIMS period. In Figure 2 the LIMS data show strong cooling in the upper stratosphere characterized by a maximum near 1.0 hPa of about 10 K/d and peaking at about 12 K/d in Northern Hemisphere polar summer. The large cooling rates (16 K/d) in the Southern Hemisphere polar summer (YAW2, YAW3) are potentially suspect because the data poleward of 64°S are not provided by the LIMS measurements as discussed above. Solar heating is characterized by a peak near the stratopause of about 11

Table 4. Global-Mean Infrared Cooling: Global Fields versus Zonally Averaged Fields

	CO_2 Cooling Rate From 500 to 850 cm^{-1} (K/d)		
Pressure, hPa	Global Field[a]	Zonally Averaged Field[b]	Difference
0.10	-2.08	-2.79	0.71
0.15	-1.63	-2.32	0.69
0.22	-1.48	-2.16	0.68
0.32	-3.99	-4.36	0.37
0.46	-7.12	-6.88	-0.24
0.68	-8.24	-7.36	-0.88
1.00	-8.08	-6.92	-1.16
1.47	-6.75	-6.17	-0.58
2.15	-5.08	-5.14	0.06
3.16	-3.83	-3.91	0.08
4.64	-2.84	-2.83	-0.01
6.81	-2.20	-2.24	0.04
10.0	-1.75	-1.82	0.08
14.7	-1.50	-1.55	0.05
21.5	-1.27	-1.28	0.01
31.6	-0.97	-0.98	0.01
46.4	-0.68	-0.69	0.01
68.1	-0.31	-0.33	0.01
100.	-0.02	-0.04	0.02

[a] Global fields of Microwave Limb Sounder MLS-observed temperature were used to calculate cooling rates from CO_2 in the 500-850 cm^{-1} region. Cooling rates were calculated using every level 3AT temperature profile available from the DAAC during UARS YAW3 period (28 UARS days, 36,914 temperature profiles). The cooling rates were then zonally averaged and then globally averaged.

[b] Zonally averaged fields of Microwave Limb Sounder MLS-observed temperature were used to calculate cooling rates from CO_2 in the 500-850 cm^{-1} region. Zonal-mean temperature profiles were calculated from every level 3AT temperature profile available from the DAAC during UARS YAW3 period. Zonal-mean cooling rates were calculated next and then global-mean cooling rates.

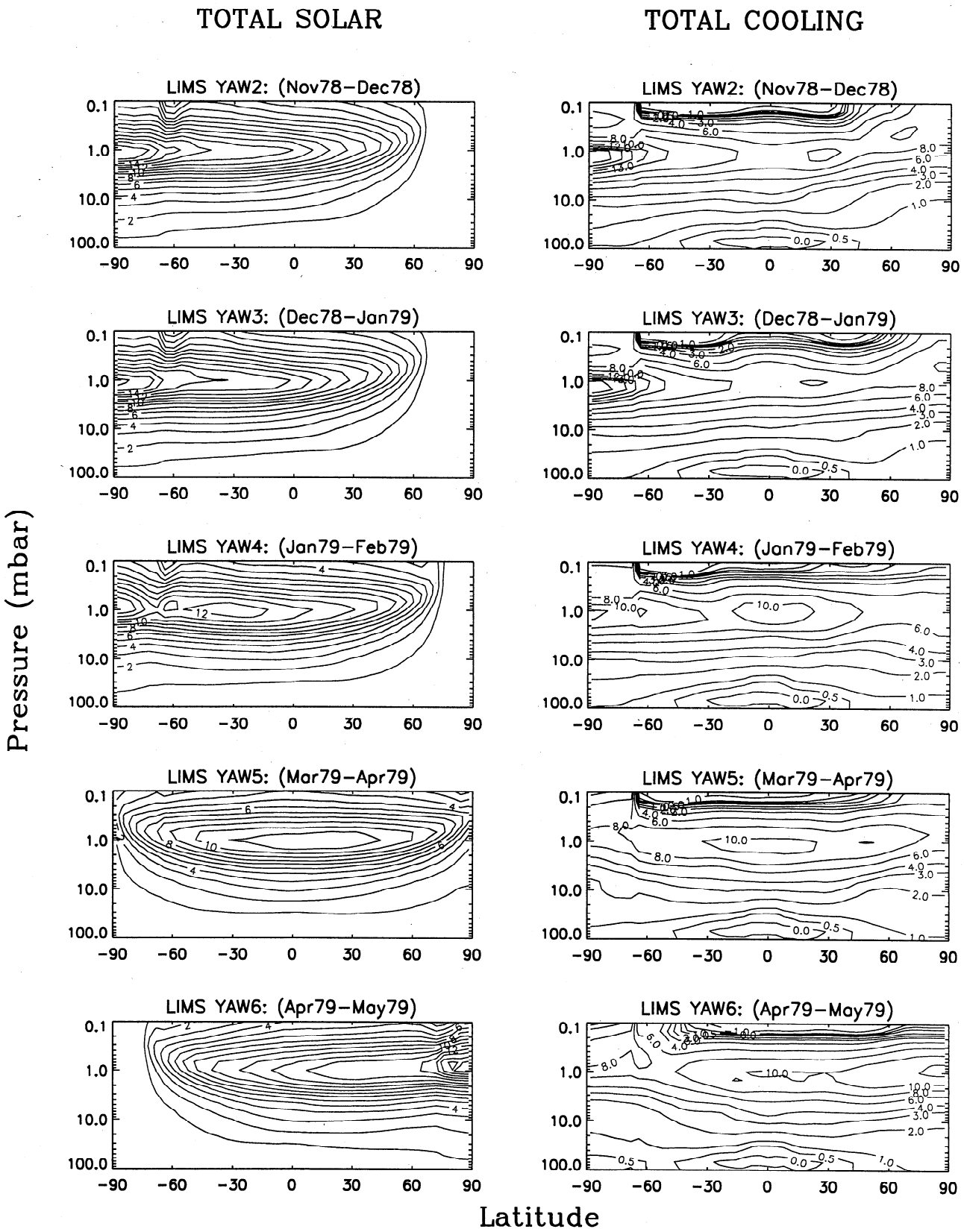

Figure 2. Total solar heating and total infrared cooling (K/d) calculated from LIMS data.

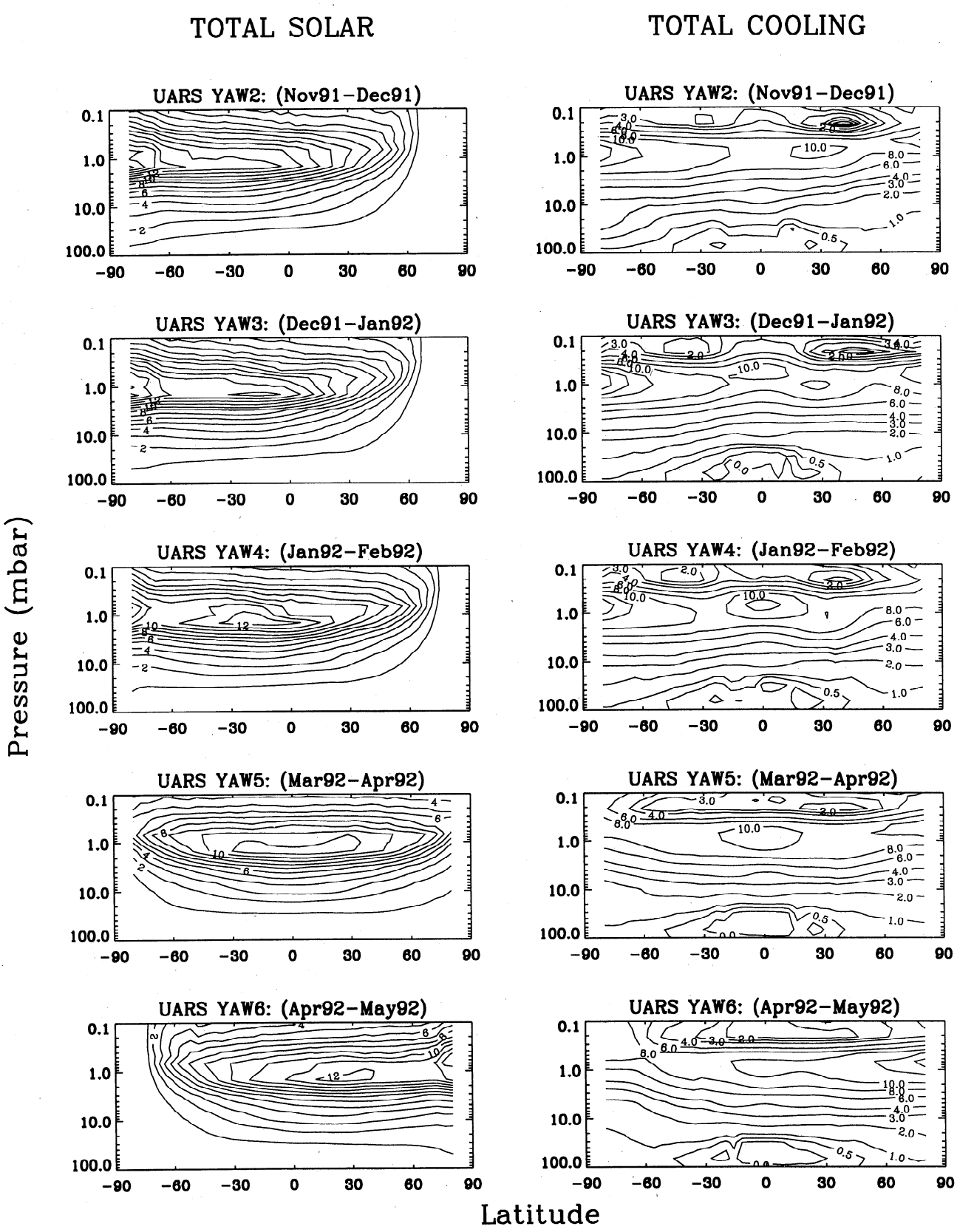

Figure 3. Total solar heating and total infrared cooling (K/d) calculated from UARS data.

K/d at equinox (YAW5) with values exceeding 12-14 K/d during polar summer. The march of seasons is clearly evident in the progression of infrared cooling and solar heating.

The total solar heating and infrared cooling from the UARS period are plotted in Figure 3. While many of the same climatological features are present in both LIMS and UARS data sets, there are noticeable and

important differences between the two. These differences will also be reflected in the diagnosed meridional and vertical circulations presented below. For example, the UARS data on total infrared cooling in Figure 3 exhibit a maximum cooling of about 11 K/d peaking in altitude above the stratopause at about 0.7 to 0.8 hPa. This is in contrast to the LIMS data which generally peaks around 10 K/d near the stratopause and at about 1.0 hPa or just higher (lower) in pressure (altitude). The height of the cooling peak in the UARS data may be partially determined by the joining of the Microwave Limb Sounder temperatures and the NMC temperature climatology which occurs at approximately 0.46 hPa. The effects on the calculated cooling rate of any discontinuities in the temperature profile are manifest several kilometers below and above the discontinuity, as previously discussed. The total solar heating in Figure 3 from UARS is about the same magnitude as in LIMS but generally peaks at a higher pressure (or lower altitude) at 1.5 hPa. The height in the solar heating peak is determined by the height of the peak in the daytime-averaged ozone concentration. The ozone concentration from the Microwave Limb Sounder peaks at a higher pressure as compared to LIMS.

The net diabatic heating rates computed from the solar and infrared rates above (total solar heating minus total infrared cooling) are presented in Plate 2, along with net diabatic heating rates for the remaining UARS periods (YAW1 and YAW7-YAW13). Below we compare the net diabatic heating rates between LIMS and UARS for YAW2-YAW6. It is evident that the entire tropical and midlatitude stratosphere experiences a net heating (more solar heating than infrared cooling) for latitudes primarily between 40°S and 40°N. There is also net heating in the polar regions during summer and net cooling in the polar regions during winter, illustrating the departures from radiative equilibrium at those locations and times. These results are consistent with the work of MG, KS, and *Gille and Lyjak* [1986]. Perhaps the most readily apparent difference between LIMS and UARS in these figures is in the net heating which is in general stronger for UARS than for LIMS. In particular, there is strong net heating during UARS YAW3 exceeding 5 K/d in the tropical upper stratosphere. Just above this maximum in heating near 0.3 to 0.6 hPa in the tropics there is actually net cooling in UARS YAW3. Evidence of two local maxima in net heating near 40°N and 40°S is present in both LIMS and UARS. These maxima are located near 0.2 to 0.3 hPa. By equinox (YAW5) there is evidence of a pair of weaker maxima near 30°S and 30°N near the stratopause, especially in UARS data.

3.2. Global Radiation Balance

It is believed that the stratosphere should approach radiative equilibrium over seasonal timescales when the net radiative heating is horizontally averaged over the globe on each pressure surface. *Olaguer et al.* [1992] have shown that on a monthly basis the infrared cooling and solar heating should be in balance to within 0.03 K/d. Validating the equilibrium state of the stratosphere places stringent accuracy requirements on both the radiation transfer algorithms and the remote measurement techniques. Radiation transfer algorithms have only recently achieved these accuracies, as demonstrated for our infrared radiation models in paper 1. Global observations of the atmospheric state are not yet so accurate. *Olaguer et al.* [1992] also showed that distributions of important chemical tracers are sensitive to diabatic heating differences larger than 0.1 K/d in the lower stratosphere. Therefore the calculated global radiation balance should be maintained at least to within 0.1 K/d. We demonstrate in this section that the global radiative balance in the stratosphere is nearly within 0.1 K/d when computed from the LIMS and UARS data sets. This balance is achieved without any prior "adjustment" of the data as was done, for example, by *Kiehl and Solomon* [1986], *Gille and Lyjak* [1986], and *Pawson and Harwood* [1989].

Figure 4 shows the globally averaged infrared cooling, solar heating, and net diabatic heating during both LIMS and UARS periods for YAW2-YAW6 (November-December to April-May). The radiative imbalance at each UARS pressure level is given in Table 5 for YAW3 (December to January), which is representative of all yaw periods. The radiative imbalance is almost always within 0.1 K/d in the lower stratosphere from ~30 to 70 hPa and nearly within 0.1 K/d at 100 hPa. Considering the entire stratosphere from 1 to 100 hPa, two-thirds of the pressure levels are within 0.2 K/d. Below we show that the calculated global-mean radiative imbalance is largely explained in terms of the uncertainty in input atmospheric data, and the agreement between global-mean solar heating and global-mean infrared cooling presented in Figure 4 and Table 5 is the closest achieved to date. The imbalance is much larger in the mesosphere where the errors in the infrared cooling rate calculations and in the measurements increase (see UARS validation papers). The radiation fields calculated using UARS data are closer to a globally averaged balance than those calculated using LIMS data. This is mainly due to advances in molecular spectroscopy since the time of the original LIMS processing. Because of improvements in the molecular line database (i.e., HITRAN) the LIMS globally averaged net radiative heating rates in Figure 4 are much closer to radiative balance than reported by *Kiehl and Solomon* [1986], where the globally averaged solar heating and infrared cooling generally differed by no more than 25% throughout the stratosphere. Our calculations predict that solar heating and infrared cooling agree in the stratosphere to better than 12% (see Table 5) in regions where the UARS data are generally considered to be scientifically useful (22 hPa to 0.46 hPa).

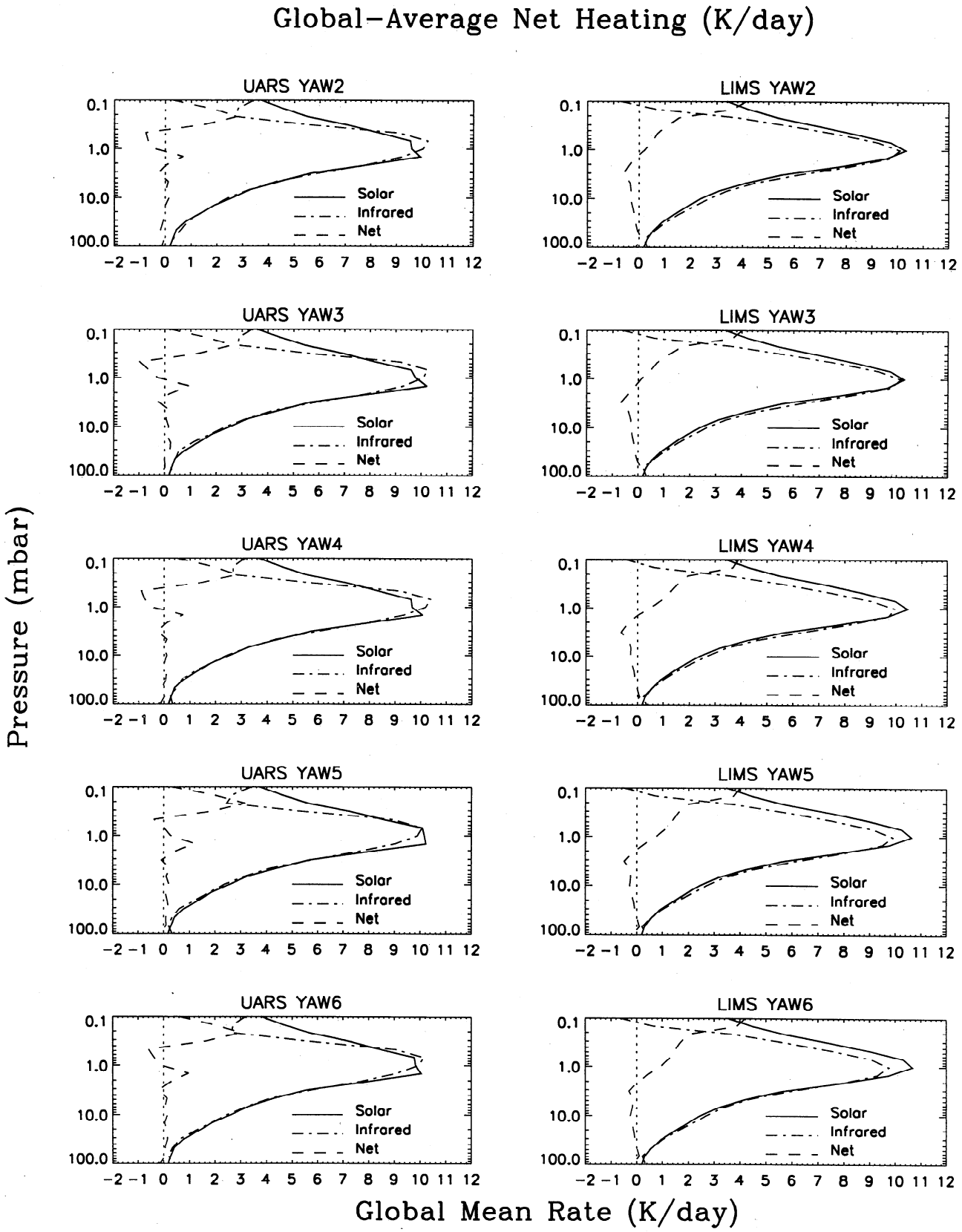

Figure 4. Monthly global-average heating rates for LIMS and UARS. Months are UARS yaw periods concomitant with LIMS. Heating rates shown are solar heating, infrared cooling, and net diabatic heating (or radiative imbalance).

Table 5. Global-Mean Net Diabatic Heating and Percent Radiative Imbalance for YAW3

	Rate Imbalance (K/d) and Percent Imbalance (%)					
	UARS (aer)[a]		UARS (noacr)[b]		LIMS	
Pressure, hPa	Rate	%	Rate	%	Rate	%
0.10	0.10	3	0.06	2	3.95	120
0.15	1.56	35	1.53	34	3.63	85
0.22	2.54	47	2.53	47	1.65	31
0.32	1.20	17	1.20	17	1.09	16
0.46	-1.05	-13	-1.04	-13	0.65	8
0.68	-0.65	-7	-0.65	-7	0.46	5
1.00	-0.28	-3	-0.28	-3	0.13	1
1.47	0.86	8	0.86	8	-0.22	-2
2.15	0.10	1	0.10	1	-0.49	-6
3.16	-0.25	-4	-0.26	-5	-0.69	-12
4.64	0.13	3	0.12	3	-0.45	-11
6.81	0.05	1	0.03	1	-0.29	-9
10.0	0.16	6	0.11	4	-0.28	-12
14.7	0.00	0	-0.13	-7	-0.30	-17
21.5	0.15	12	-0.18	-14	-0.23	-18
31.6	0.21	27	-0.22	-29	-0.13	-15
46.4	-0.01	-2	-0.29	-72	-0.04	-7
68.1	0.03	11	-0.07	-25	0.11	35
100.	-0.15	-88	-0.19	-112	-0.17	-100

[a] Pinatubo aerosols included.
[b] Pinatubo aerosols not included.

We now assess the impact of the uncertainties in the model calculations and the observed temperature and gas concentrations on the global radiative balance. Figure 5 contains plots of the global-mean solar heating, infrared cooling, and net diabatic heating for LIMS and UARS YAW3. We choose YAW3 (December to January) because this month had the best global coverage of Pinatubo aerosols by the HALOE instrument during peak aerosol loading. The stratosphere is in perfect global-mean radiative equilibrium in steady state if the global-mean net diabatic heating is identically zero. On monthly timescales, however, the stratosphere should be in radiative balance to within ±0.03 K/d [*Olaguer et al.*, 1992]. From Figure 5 and Table 5 the calculated global-mean net diabatic heating, or radiative imbalance, exceeds ±0.03 K/d at most pressure levels within

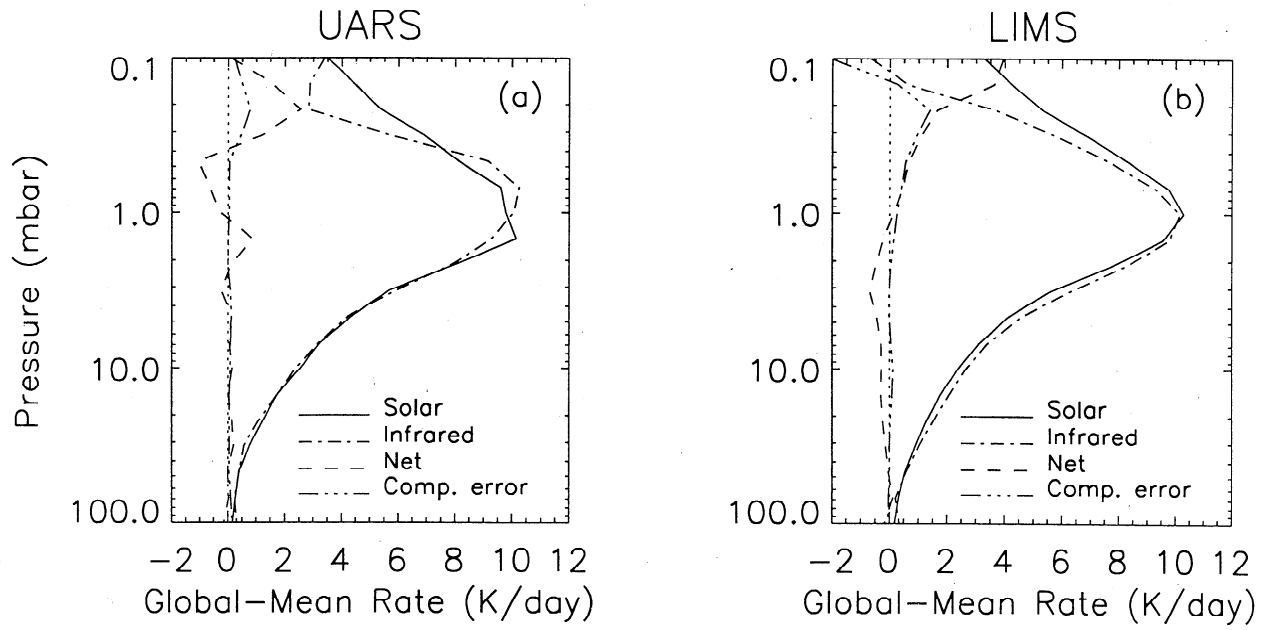

Figure 5. Comparison of global-average radiative imbalance with estimated uncertainty in infrared cooling rate calculation for (a) LIMS and (b) UARS YAW3.

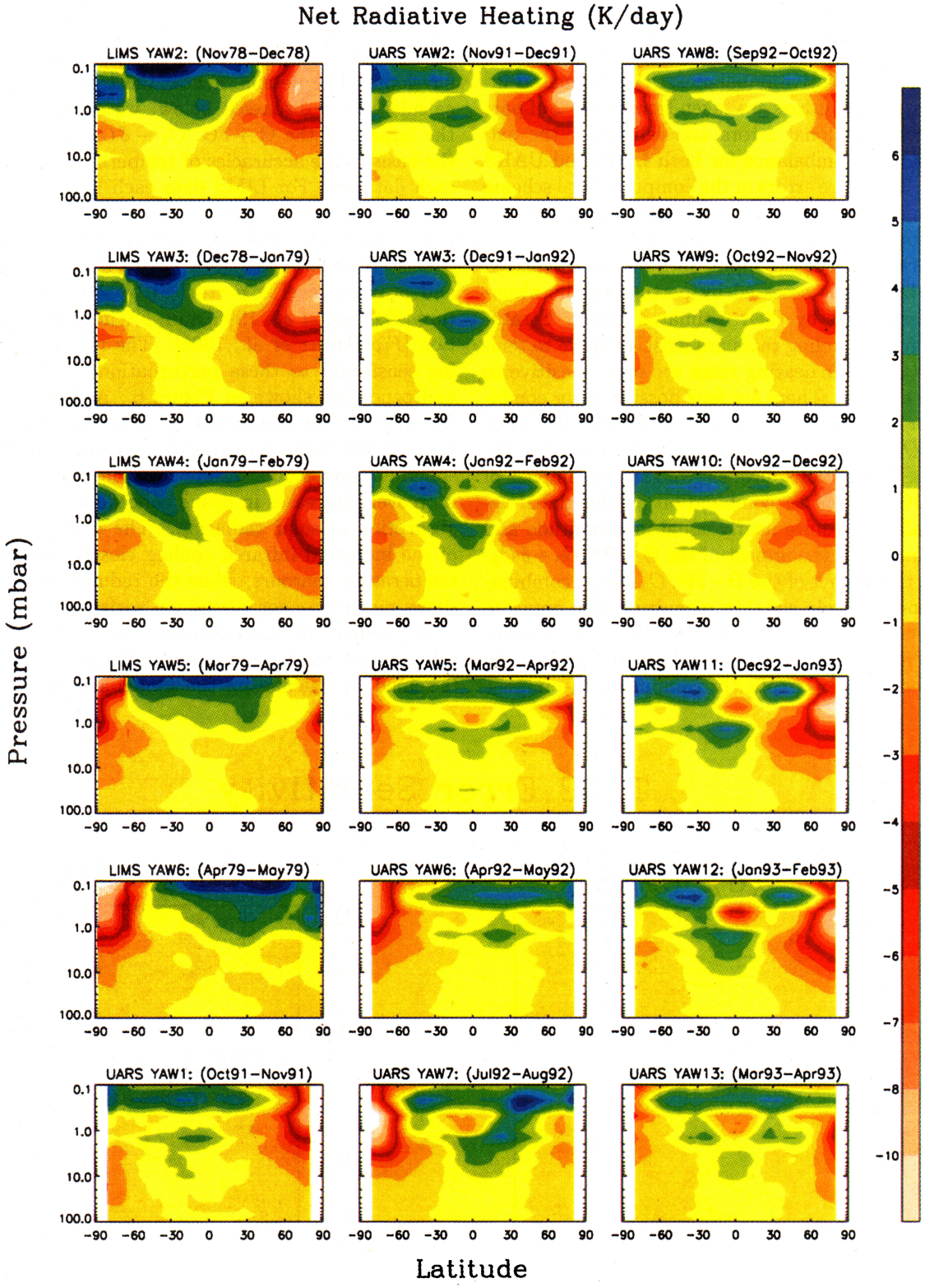

Plate 2. Net radiative heating (K/d) calculated from LIMS and UARS data.

the stratosphere. Overlaid on the plots in Figure 5 are profiles of the infrared cooling rate difference between the LPK and the EGA models (see part 1) to see if the computational uncertainty can account for the calculated radiative imbalance. The estimated infrared cooling rate errors are taken from Table 2 of part 1. The computational errors are well below the calculated radiative imbalance for both LIMS and UARS data sets. Therefore errors in the computational scheme alone cannot account for the calculated imbalance between global-mean heating and cooling.

The uncertainty of the input data on the calculated radiative balance is assessed by perturbing the atmospheric parameters by their estimated errors. Stratospheric infrared cooling rates are most sensitive to temperature (Θ); solar heating rates are most sensitive to the ozone amount. There are four possible error combinations for the two input parameters: $\Theta+\delta\Theta$, $O_3+\delta O_3$; $\Theta-\delta\Theta$, $O_3-\delta O_3$; $\Theta+\delta\Theta$, $O_3-\delta O_3$; and $\Theta-\delta\Theta$, $O_3+\delta O_3$. Simulations have shown that the impact of the $\Theta-\delta\Theta$, $O_3-\delta O_3$ combination on the global radiation balance is quite nearly equal in magnitude and opposite in sign to the impact of the $\Theta+\delta\Theta$, $O_3+\delta O_3$. Similarly, the impact of the $\Theta-\delta\Theta$, $O_3+\delta O_3$ combination is approximately equal in magnitude and opposite in sign to the impact of the $\Theta+\delta\Theta$, $O_3-\delta O_3$ combination. Thus two independent error envelopes can be constructed: one by explicitly computing the impact of the $\Theta+\delta\Theta$, $O_3+\delta O_3$ combination and taking the negative to form one envelope; the second by explicitly computing the impact of the $\Theta+\delta\Theta$, $O_3-\delta O_3$ combination and taking the negative to form the other error envelope. The details of how the error envelopes are calculated are discussed below; we explicitly consider the impact of the $\Theta+\delta\Theta$, $O_3-\delta O_3$ combination on the basis of the accuracies of temperature and ozone in each data set. For LIMS data each latitude and pressure level in YAW3 is perturbed by 2.0 K in temperature [*Gille et al.*, 1984] and -20% in ozone concentration [*Remsberg et al.*, 1984]. For UARS data, each latitude and pressure level is perturbed by 4.0 K in temperature [*Fishbein et al.*, 1996] and -5% in ozone concentration [*Froidevaux et al.*, 1996]. The net diabatic heating sensitivity to these perturbations in temperature and ozone are shown in Figure 6. A similar sensitivity analysis was conducted by *Gille and Lyjak* [1986] using LIMS data. As expected, an increase in stratospheric temperatures results in an increase in cooling. Moreover, decreases in ozone concentration reduce the absorption of solar radiation. The contour structure of the increased infrared cooling closely resembles the temperature contours, while the reduced solar heating shows much stronger latitudinal variations.

The impact of the uncertainty in the input atmospheric data on the computed radiative balance is determined by calculating the global-average change in

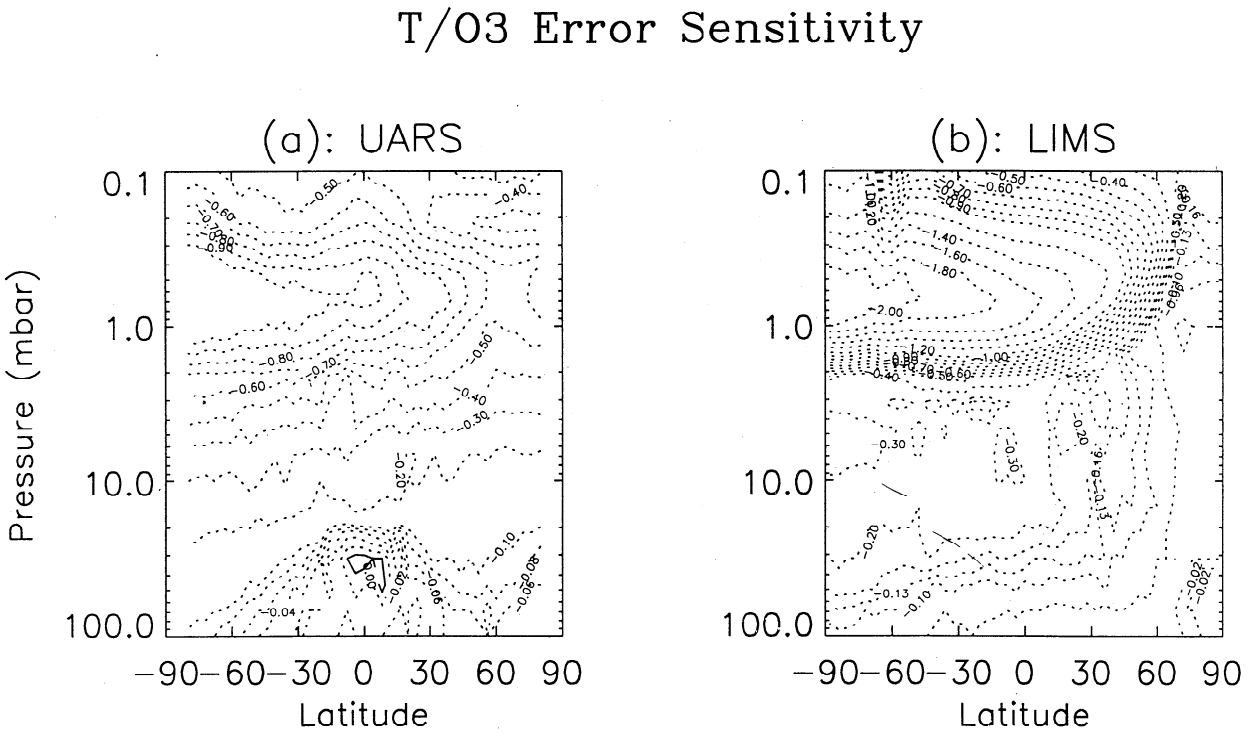

Figure 6. Net diabatic heating rate differences in (a) LIMS and (b) UARS YAW3 between perturbed and unperturbed input atmospheric data. The unperturbed temperatures were increased by 2 K for LIMS and 4 K for UARS. The unperturbed ozone concentrations were decreased by 20% for LIMS and 5% for UARS. See text for details.

net diabatic heating (shown in Figure 6) due to the estimated errors in both the temperature and the ozone amount. This quantity is compared in Figure 7 to the radiative imbalance for YAW3 (December to January) during both LIMS and UARS periods. Figure 7 is a plot similar to the comparison between the radiative imbalance and the estimated computational error shown in Figure 5. For UARS data (Figure 7a) the estimated input data errors account for most of the radiative imbalance in the stratosphere at pressures below 20 hPa. The imbalance in the lower stratosphere is likely to be caused by increasing errors in the measured atmospheric parameters in the lower stratosphere (see UARS validation papers) and possibly an overestimation of the infrared heating by Pinatubo aerosols by assuming clear-sky conditions (see part 1). The impact of clouds on stratospheric radiative heating is discussed in part 1. The radiative imbalance in the lower stratosphere during UARS can also be due to the fact that the measured data become mostly climatological at pressures higher than 20 hPa (see Table 2). The input error envelope in Figure 7a is almost identical for the two independent error combinations discussed in the preceding paragraph. For LIMS data, however, the two error combinations produce very different error envelopes. The $\Theta + \delta\Theta$, $O_3 + \delta O_3$ combination (not shown) does not come close to explaining the radiative imbalance, while the $\Theta + \delta\Theta$, $O_3 - \delta O_3$ combination, shown in Figure 7, nearly explains the radiative imbalance throughout most of the stratosphere. As stated at the beginning of this section, the imbalance in the LIMS data is probably due to the older molecular spectroscopic data available at the time of the original LIMS processing. The LIMS data are presently being reprocessed with updated spectroscopic parameters. The ozone amounts near 2-3 hPa are expected to increase by about 5% (E. Remsberg, private communication, 1998). This increase will reduce the peak discrepancy between solar heating and infrared cooling in the upper stratosphere LIMS data. However, we emphasize that the LIMS radiative imbalance has been significantly reduced compared to the work of KS, by a factor of 2 or more, and is near the imbalance criteria put forth by *Olaguer et al.* [1992].

Figure 8 shows the global-average net diabatic heating for UARS YAW3 with and without Pinatubo aerosols included. The data are also given in Table 5. The presence of the aerosol layer had a significant effect on the lower stratospheric radiative energy budget. One can clearly see from Table 5 that the percent imbalance was greatly reduced by including infrared emission and absorption by Pinatubo aerosols. Pinatubo aerosols added as much as 0.43 K/d to the global-average net diabatic heating at 31.6 hPa in YAW3. Although not shown here, the maximum radiative effect remained at 31.6 hPa until YAW7 (July-August 1992), where it dropped to 46.4 hPa with an added 0.27 K/d to the global-average net diabatic heating. A maximum heating by Pinatubo aerosols of 0.23 K/d occurred at 68.1 hPa during YAW8 (September-October 1992). The maximum heating added remained at 68.1 hPa from YAW8-YAW13 (September 1992 to April 1993) where 0.14 K/d was added in YAW13.

To further assess the global energy balance of the stratosphere, we have also calculated the total energy gained by the entire stratosphere due to absorption of solar radiation and the total energy lost by the stratosphere due to emission of infrared radiation. The goal is to see whether or not our calculations indicate a balance between absorbed and emitted energy within the entire stratospheric system. These calculations are similar to

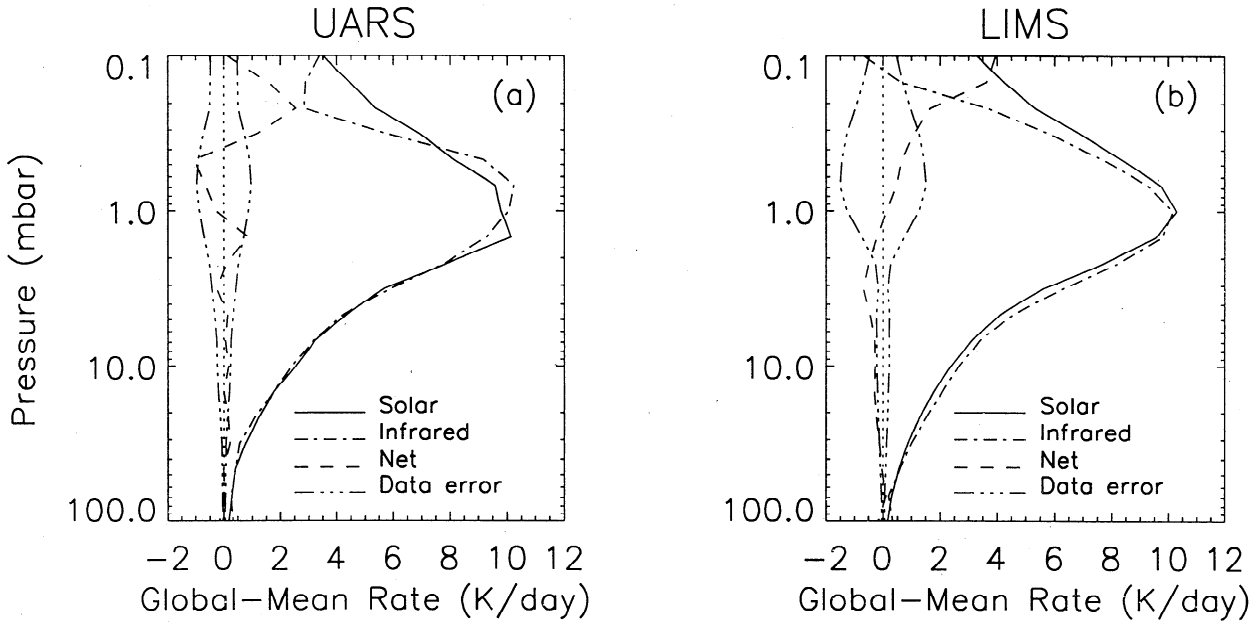

Figure 7. Comparison of global-average radiative imbalance with estimated uncertainty in input atmospheric data for (a) LIMS and (b) UARS YAW3.

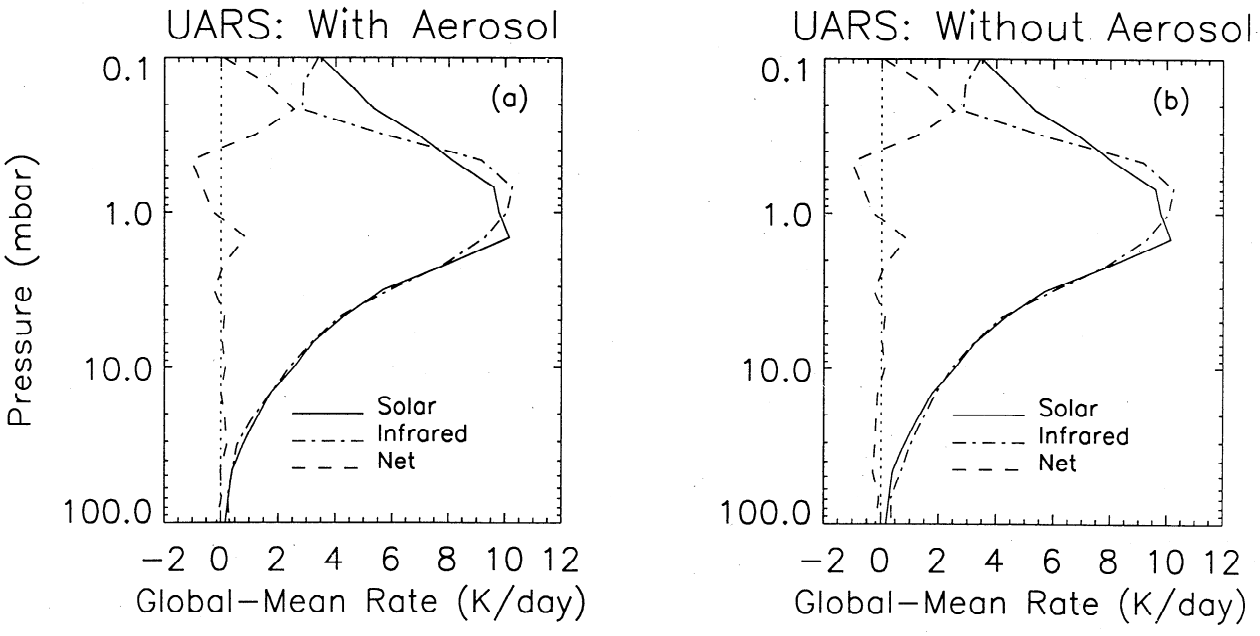

Figure 8. Global-average heating rates for UARS YAW3 (a) with and (b) without Pinatubo aerosols included.

those routinely carried out in studies of the Earth radiation budget in which the zonally averaged absorbed solar energy is compared with the zonally averaged energy emitted by the planet [e.g, *VonderHaar and Suomi*, 1971]. To calculate the rate of absorption of solar energy and the rate of emission of infrared energy, we employ the first law of thermodynamics

$$\frac{\delta Q}{\delta t} = \rho c_p \frac{\delta \Theta}{\delta t} \tag{2}$$

which gives the local rate of energy gain or loss per unit volume ($\delta Q/\delta t$). Integrating this expression with respect to height (and employing hydrostatic equilibrium) yields the total rate of energy gain or loss $E(\theta)$ per unit area within the vertical region of atmosphere defined by the limits of integration; that is,

$$\begin{aligned} E(\theta) &= \int_z \frac{\delta Q}{\delta t} dz = \int_z \rho c_p \frac{\delta \Theta}{\delta t} dz \\ &= -\frac{c_p}{g} \int_p \frac{\delta \Theta}{\delta t} dp \end{aligned} \tag{3}$$

where Θ is temperature and the heating rates $\delta\Theta/\delta t$ are functions of latitude (θ) and pressure. Total absorbed solar energy and the total emitted infrared energy are determined by carrying out the integration using the solar heating rates and infrared cooling rates given above. For this study we nominally define the "stratosphere" to be the region between 1 and 100 hPa.

Figure 9 shows $E(\theta)$ plotted versus the sine of latitude so that the abscissa is proportional to area. The solid line represents the rate of absorption of energy from solar radiation, and the dashed line is the rate of loss from infrared emission. The $E(\theta)$ shown in the figure are from YAW13 (March, equinox) and YAW11 (January, Northern Hemisphere winter) from the UARS data. It is clear that the stratosphere gains more energy than it loses at low latitudes, and it loses more energy than it gains at high latitudes. The curves cross at 32°S and 36°N in March and at 44°S and 24°N in January. Despite the length of day in the Southern Hemisphere summer (January) the polar stratosphere, as a whole, continually loses more energy than it gains.

The global balance of heating and cooling in the stratosphere can also be assessed by evaluating the (area weighted) global mean of $E(\theta)$. These values are given in Table 6 for the 13 UARS months and for the 5 LIMS months. Without any adjustment we find that the total, global-mean energy absorbed by the stratosphere and the total global-mean energy emitted by the stratosphere to balance, on average, to better than one-half (0.5) percent for the 13 UARS months. The area under the individual curves in Figure 9 are identical to within about 1.5%. The balance is not so good during the 5 LIMS months as we find the global mean of $E(\theta)$ to balance to about 8%, with the energy loss computed to be larger than the energy absorbed. Comparison of the UARS and LIMS values in Table 6 show that the absorbed solar energy is about the same during UARS and LIMS, suggesting that the LIMS energy loss may be too large. The global mean temperature profiles for the 5 months common to LIMS and UARS are larger by about 1-3 K during LIMS than UARS over the 1 hPa to 100 hPa range, causing the larger calculated stratospheric loss during the LIMS period. *Remsberg et al.* [1994] noted that the LIMS temperatures are slightly too warm in the middle and upper stratosphere. Nevertheless, this analysis conclusively demonstrates that the entire stratosphere as a thermodynamic entity is very

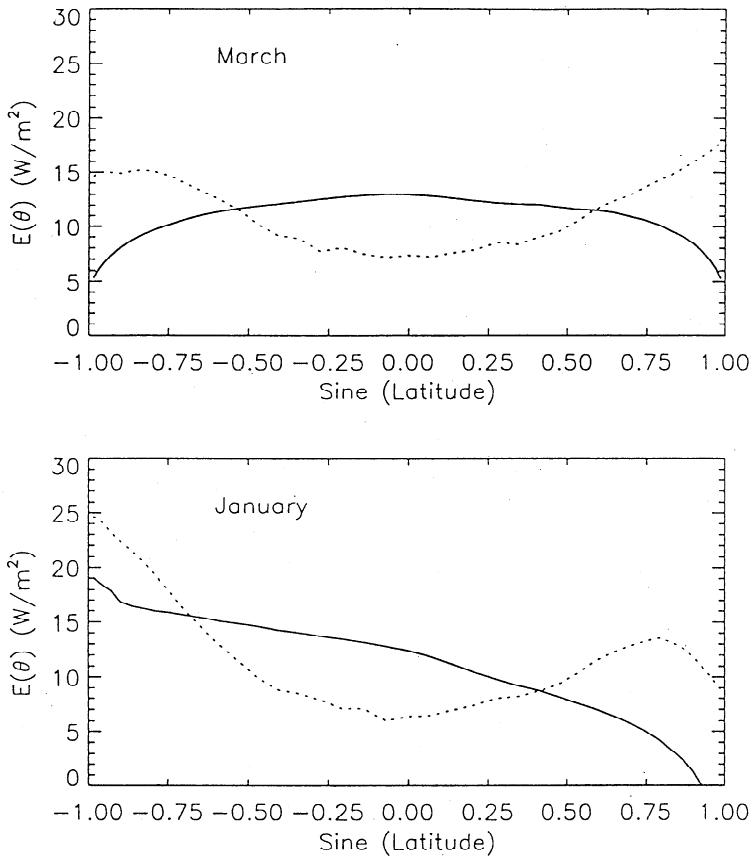

Figure 9. Absorbed solar energy (solid line) and emitted infrared energy (dashed line) by the atmosphere between 1 hPa and 100 hPa (in W/m^2).

close to radiative equilibrium over monthly to seasonal periods.

3.3. Diabatic Circulation

One of the goals of this work is to calculate accurately the net radiative heating in the stratosphere in order to calculate the diabatic circulation from the computed fields of net radiative heating. As discussed in section 1, *Dunkerton* [1978] has shown that the Lagrangian-mean meridional circulation can be approximated satisfactorily by the diabatic circulation, which is obtained from the Eulerian-mean diabatic heating and temperature structure. In this section we present computations of the diabatic circulations for the LIMS and UARS data sets, and we illustrate differences between the two. We follow the formalism of *Solomon et al.* [1986a] in developing the expressions for the components w^* (mean vertical velocity) and v^* (mean meridional velocity) of the diabatic circulation.

Specifically, we calculate the mean vertical velocity w^* from the thermodynamic equation

$$w^* = \frac{Q_{\text{net}} - v^*(\partial T/\partial y) - (\partial T/\partial t)}{(\Gamma_d - \Gamma)} \tag{4}$$

where Q_{net} is the net radiative heating (zonally averaged solar heating minus infrared cooling), v^* is the mean meridional velocity, $\partial T/\partial y$ is the zonally averaged meridional temperature gradient, and $\partial T/\partial t$ is the zonal mean local rate of change of temperature. The product $v^*\partial T/\partial y$ represents the meridional advection of temperature. The term $(\Gamma_d - \Gamma)$ represents the static stability in terms of the difference between the dry adiabatic lapse rate (Γ_d) and the lapse rate (Γ) of the zonally averaged temperature. Typically, Q_{net} is the largest of the three terms in the numerator, but the other two terms can be as large as 10% of the net radiative heating.

The meridional velocity v^* is derived by integrating the continuity equation

$$\frac{1}{a\cos\theta}\frac{\partial}{\partial\theta}(v^*\cos\theta) + \frac{1}{\rho}\frac{\partial}{\partial z}(\rho w^*) = 0 \tag{5}$$

where a is the Earth's radius, θ is latitude, ρ is density, and z is altitude. Because v^* appears in the expression for w^*, these equations are solved iteratively [e.g., *Solomon et al.*, 1986a; *Gille et al.*, 1987]. We also impose the constraint

$$\int_{-\frac{\pi}{2}}^{+\frac{\pi}{2}} w^*\cos\theta\, d\theta = 0 \tag{6}$$

to assure mass balance on a pressure surface and to force

Table 6. Total Energy Absorbed and Emitted by the Stratosphere Between 1 and 100 hPa

	UARS			LIMS		
	Absorbed Solar	Emitted Infrared	%Diff[a]	Absorbed Solar	Emitted Infrared	%Diff[a]
YAW1	11.51	12.92	12.3			
YAW2	11.44	12.37	8.1	11.53	12.78	10.8
YAW3	11.15	10.82	-3.0	11.51	12.68	10.2
YAW4	11.21	11.50	2.6	11.48	12.56	9.4
YAW5	11.27	10.52	-6.7	11.69	12.52	7.1
YAW6	11.32	10.81	-4.5	11.88	12.52	5.4
YAW7	11.21	10.16	-9.4			
YAW8	11.20	10.33	-7.8			
YAW9	11.24	11.06	-1.6			
YAW10	11.17	11.21	0.4			
YAW11	11.07	11.25	1.6			
YAW12	11.03	11.29	2.4			
YAW13	11.18	11.02	-1.4			
Average	11.23	11.17	-0.5	11.62	12.61	8.5

[a] %Diff: 100x(emitted infrared - absorbed solar)/absorbed solar

v^* to zero at the poles. This constraint also effectively forces global mean radiative equilibrium. The term w^* is first evaluated according to (4) as a function of latitude with v^* set equal to zero. An adjusted vertical velocity is then determined by subtracting the global mean value of w^* calculated from (6). This "adjusted" vertical velocity is then used in (5) to compute v^*. The process converges in a few interations, and five iterations are used in all cases. As stated previously, these adjustments are much smaller than required in previously published studies due to the near achievement of global radiative equilibrium. As discussed above, our radiative calculations show the stratosphere to be very close to radiative equilibrium on a monthly timescale. We have not adjusted our radiative calculations prior to computing the diabatic circulations as was necessary in the studies of *Kiehl and Solomon* [1986], *Gille et al.* [1987], and *Eluszkiewicz et al.*, [1996, 1997]. Any adjustment required to achieve mass balance is carried out during the calculation of the circulations through application of the above constraint, similar in fashion to the previous studies, and is quite small.

Plate 3 shows the values of w^* for the LIMS and UARS periods and in Plate 4 the corresponding values for v^*. In the following discussion we compare the diabatic circulation patterns between LIMS and UARS periods for YAW2-YAW6. There are strong similarities between the patterns of vertical velocity in the months common to LIMS and UARS (mid-November through mid-May) despite the 13 year separation between the two sets of observations. Common features in the data for YAW2 through YAW4 (December-February) include rising motion throughout the tropical stratosphere and into the lower mesosphere; the axis of this upwelling region slopes toward the summer hemisphere and reaches a maximum near 0.3 hPa and 30°S. In the midlatitudes of the winter hemisphere (poleward of about 40°N), both data sets show descending motion; this downwelling becomes more intense during February (YAW4), especially in the LIMS data, before weakening in March (YAW5). *Solomon et al.* [1986a] argued that the pattern of ascending motion in the subtropics of the summer hemisphere and descent in the middle latitudes of the winter hemisphere reflects the influence of planetary wave driving, which forces such a global circulation. In particular, the strong descent seen during YAW4 of the LIMS data set is apparently the result of enhanced wave driving associated with the stratospheric sudden warming of February 1979.

In the tropical lower mesosphere a region of descending motion is seen during YAW2-YAW3 (November-January) in both UARS and LIMS data, although this feature is stronger in UARS observations. During YAW4 (February) the tropical downwelling region descends to 0.6-0.7 hPa, and by YAW5 (March) it is found near the stratopause, although with much smaller amplitude (in the LIMS data there is just a minimum in upwelling rather than actual downwelling.) This descending pattern of downwelling is associated with the descending westerly phase of the stratopause semiannual oscillation; the wave forcing that drives the westerly phase generates a secondary meridional circulation with maximum downwelling just below the region of wave dissipation.

In the tropical lower stratosphere the data for YAW5 (March) also exhibit rising motion, albeit weaker than in winter months, and descending motion poleward of 35°-40°in both hemispheres. During YAW6 (April to May) the transition to the Southern Hemisphere winter regime is evident, with strengthening descent at high southern latitudes and the beginning of rising motion at high northern latitudes. The patterns of rising and

sinking motion throughout the entire period (YAW2-YAW6) are consistent with the patterns of net heating and cooling presented in Plate 2 above.

We find the computed values of w^* to be very consistent in shape and in magnitude with those reported by E1. For example, in YAW2 the zero line for vertical velocity lies at 30°N in both computations. Maximum descent in the Northern Hemisphere lower mesosphere is of the order of 8 to 10 mm/s in both cases. Maximum upwelling of 3-4 mm/s in the Southern Hemisphere lower mesosphere is also found in both cases. During YAW5 (equinox), downwelling of 1-2 mm/s occurs slightly above 1 hPa and centered at the equator. The consistency between the computations of E1 and those reported here is higher for the w^* calculations than for the v^* calculations.

In Plate 4 we show the values of v^* for LIMS and UARS periods and compare the two sets of results for YAW2-YAW6. As was the case with w^*, v^* exhibits a large degree of similarity between the two data sets, although there are some significant differences in magnitude which may reflect the natural variability of the stratosphere. The patterns of v^* reflect the predominant summer-to-winter circulation in the upper stratosphere and lower mesosphere; this circulation weakens at equinox (YAW5) and reverses as southern winter begins (YAW6). Superimposed on this pattern is a smaller-scale pattern in the tropical upper stratosphere and lower mesosphere. This pattern is associated with the semiannual oscillation and consists of equatorward motion above the tropical downwelling region described above (Plate 3) and poleward motion below. The pattern is especially apparent in YAW3-YAW4 (November to January) in the UARS data.

In comparison with the work reported by E1 we find the fields of v^* to be qualitatively consistent but with some important differences. For example, both sets of computations exhibit peaks in v^* near 1 hPa, but the values reported by E1 are typically larger in magnitude by 1 m/s or more. We also see a persistent region of negative v^* between 30 and 50 hPa in the Northern Hemisphere in the results of E1 during YAW2 through YAW6, which is not present in our calculations. Our results for the LIMS period are quite consistent with those of *Solomon et al.* [1986a] who do not indicate any negative v^* in the Northern Hemisphere lower stratosphere in January or March. We further note that the radiative effects of Pinatubo aerosols are largest in the 30 to 50 hPa layer. We suggest that the differences in v^* may be due to E1 not including aerosol radiative effects in the early months after the Pinatubo eruption.

Finally, we have computed the mass-weighted stream function to illustrate the large-scale circulation in the stratosphere for every LIMS and UARS month considered. The stream function χ is evaluated from the definition

$$\frac{\partial \chi}{\partial \theta} = \rho a \cos\theta \, w^* \tag{7}$$

by integrating the expression

$$\chi(\theta, z) = a \int_{\theta}^{\frac{\pi}{2}} \rho(\theta', z) \cos\theta' \, w^*(\theta', z) d\theta' \tag{8}$$

where the symbols are as defined above. The mass-weighted stream function is not shown here but is available from the climatology database URL given in section 4.

3.4. Radiative Relaxation Time

A simple understanding of the interaction of radiation with dynamics and chemistry can be gained by introducing the radiative relaxation time. It is easy to show from the first law of thermodynamics for an ideal gas that if the thermal structure of the atmosphere is perturbed uniformly by an amount $\delta\Theta$, then the time evolution of the temperature perturbation is given by

$$\delta\Theta(t) = \delta\Theta(0) e^{-t/\tau_{\rm rad}}. \tag{9}$$

The radiative relaxation time $\tau_{\rm rad}$ is defined as

$$\tau_{\rm rad} = \left(\frac{dQ_{\rm net}}{d\Theta} \right)^{-1}, \tag{10}$$

where $Q_{\rm net}$ is the net diabatic heating, and dynamical heating has been ignored. The relaxation time is the timescale which characterizes the effectiveness of the radiation in damping out perturbations to the thermal structure. In addition, the relaxation time is used to calculate stratospheric radiative-equilibrium temperatures in climate forcing applications [*Ramanthan*, 1976; *Ramanathan et al.*, 1989]

To first order, the radiative relaxation time defined above is dependent only on the rate of change of infrared cooling with temperature. Numerically, we calculate the infrared radiative relaxation time from a central difference estimate

$$\tau_{\rm rad} = \frac{2\delta\Theta}{Q_{\rm IR}(\Theta + \delta\Theta) - Q_{\rm IR}(\Theta - \delta\Theta)} \tag{11}$$

by perturbing the temperature profile at each latitude by $\delta\Theta = 1$ K at all pressure levels. This is the classical Newtonian cooling coefficient or infrared radiative relaxation time which describes the response time of the atmosphere to a thermal perturbation. It has been pointed out that the anticorrelation between temperature and ozone in the upper stratosphere can lead to "photochemical acceleration" of the relaxation time [*Craig and Ohring*, 1958; *Ghazi et al.*, 1979; *Pawson et al.*, 1992]. We compute the Newtonian cooling coefficient for purposes of comparison with those of KS and Gille and Lyjak. The issue of photochemical acceleration will be addressed in a future publication.

In Figure 10 we compare the infrared radiative relaxation times during LIMS and UARS YAW3 and YAW5. Similar calculations have been done by *Kiehl*

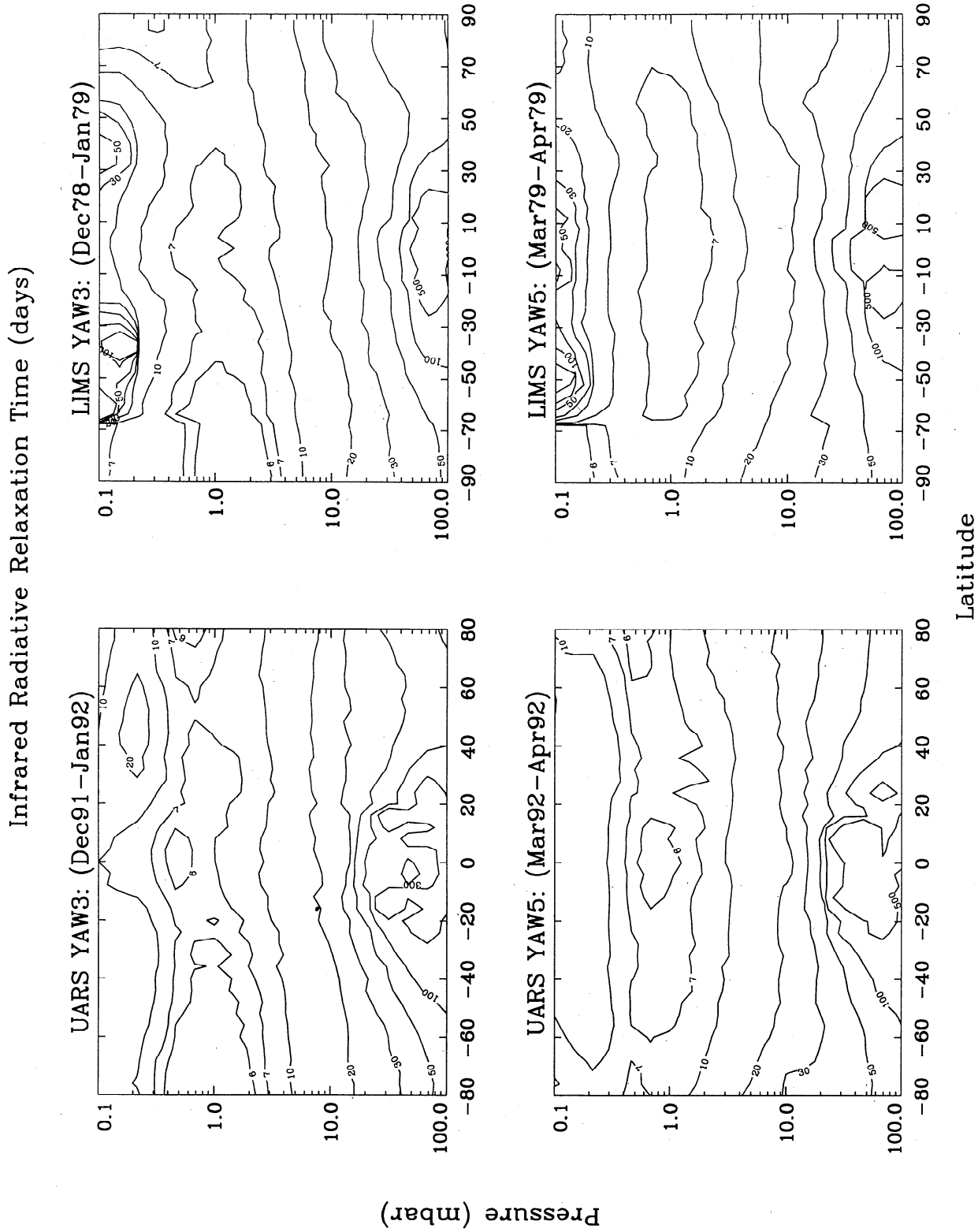

Figure 10. Infrared radiative relaxation time calculated during LIMS and UARS for YAW3 (solstice) and YAW5 (equinox).

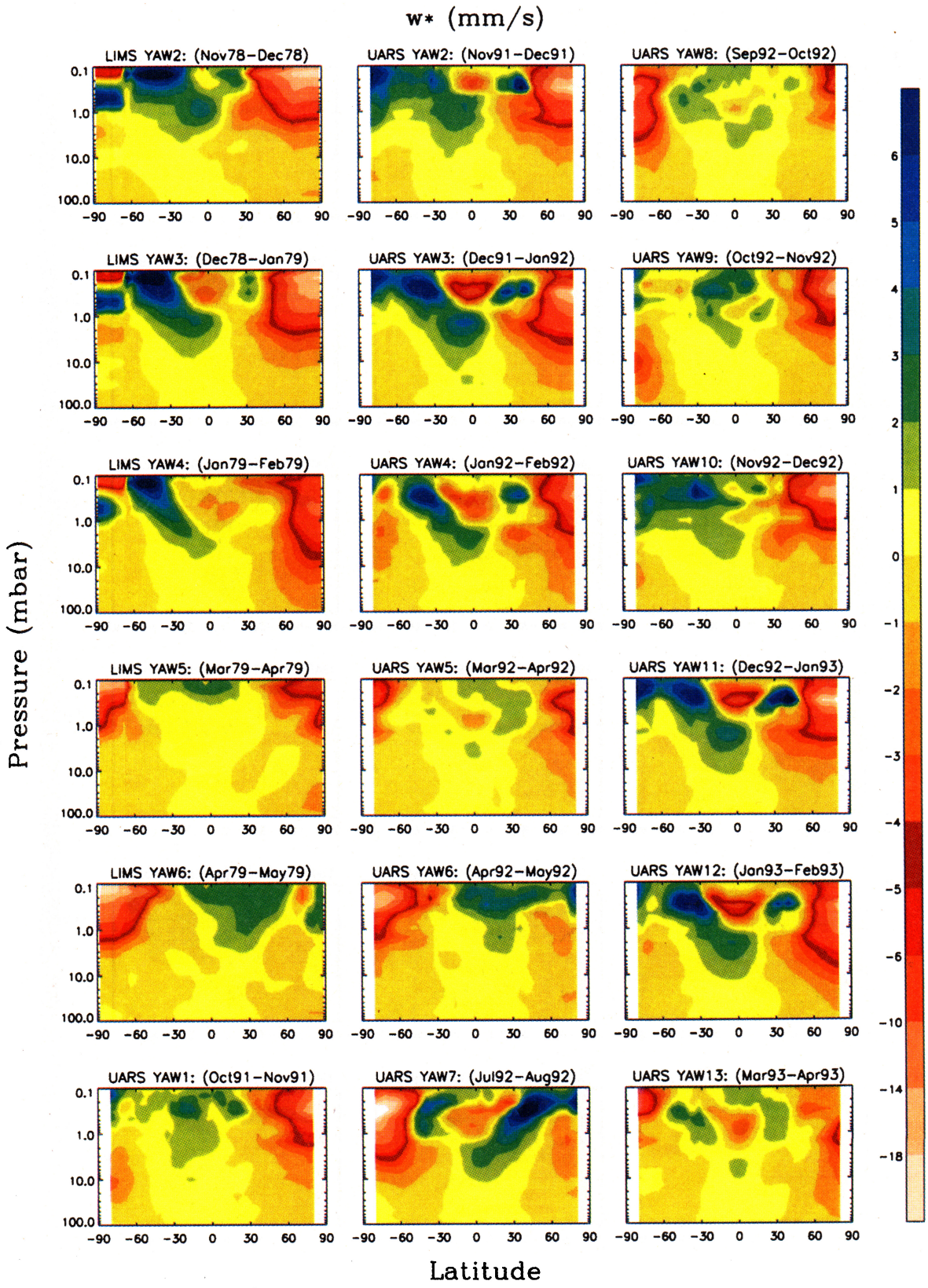

Plate 3. Mean vertical velocity derived from net radiative heating calculated from LIMS and UARS data sets.

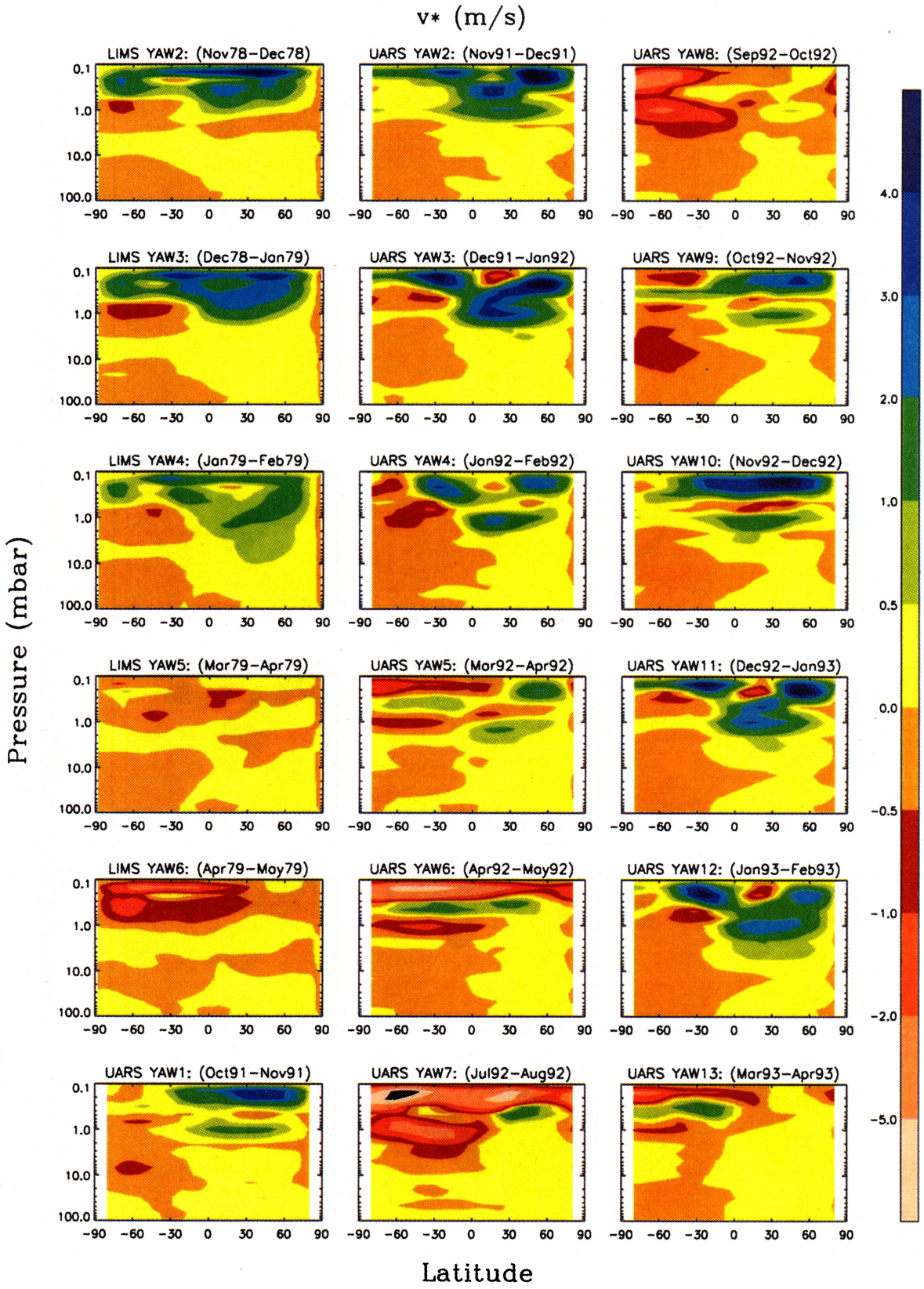

Plate 4. Mean meridional velocity derived from net radiative heating calculated from LIMS and UARS data sets.

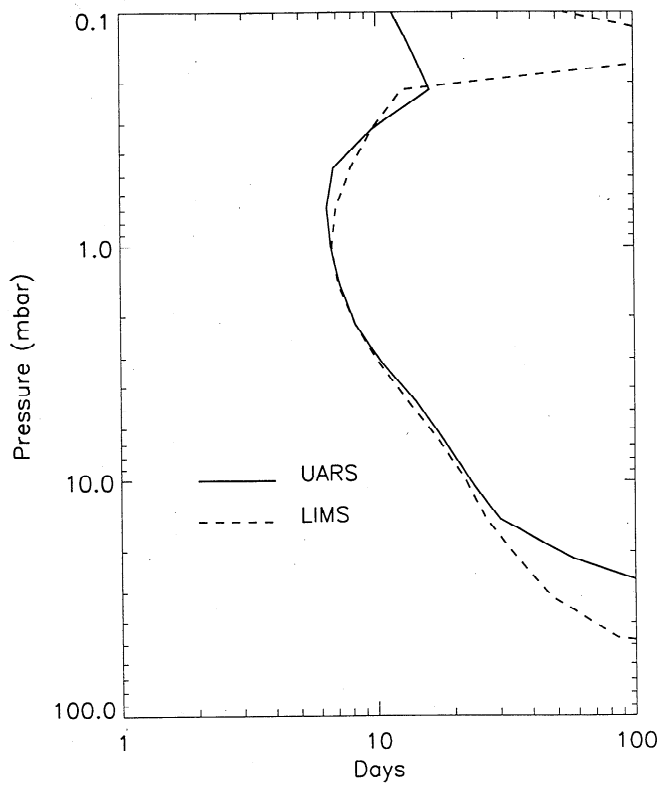

Figure 11. Globally averaged infrared radiative relaxation time calculated during LIMS and UARS for YAW3 (Dec. to Jan.).

and Solomon [1986] and *Gille and Lyjak* [1986] using LIMS data. Our results show the same qualitative features reported by them in both LIMS and UARS periods. The longest relaxation times occur near the tropical tropopause and the polar night region; the former are of the order of 80-100 days. There is a large pole-to-pole variation in the middle to upper stratosphere by roughly a factor of 2 in YAW3 (solstice). The smallest relaxation times occur at the stratopause, ~ 5-8 days, where they are comparable to planetary wave timescales. The relaxation times are fairly symmetric between the two hemispheres at equinox (YAW5). The seasonal variations at other periods are very similar between LIMS and UARS. The aerosol loading from Mount Pinatubo during UARS is noticeable in the tropical and midlatitude lower stratosphere.

Figure 11 shows globally averaged infrared radiative relaxation times during LIMS and UARS for YAW3 (December to January). The data are given in Table 7. The globally averaged relaxation times for other yaw periods and seasons show similar features. The discontinuities in the mesospheric relaxation times during UARS are due to the discontinuities in the mesospheric MLS temperature profiles where the climatology is attached. The globally averaged relaxation times are consistent between LIMS and UARS from roughly 20 hPa to 0.2 hPa. Mount Pinatubo aerosols significantly increased the globally averaged radiative relaxation time in the lower stratosphere in UARS relative to LIMS. The region most affected is between 70.0 and 30.0 hPa. For example, consider the data in Table 7. The calculated globally averaged radiative relaxation times agree to about ± 10% between LIMS and UARS without aerosols included. When Pinatubo aerosols are included in UARS, the globally averaged relaxation times are increased relative to LIMS by 62%, 100%, and 260% at

Table 7. Global Mean Radiative Relaxation Times for YAW3

	Relaxation Time (days)		
Pressure, hPa	UARS (aer)[a]	UARS (noaer)[b]	LIMS
0.10	11.6	11.4	53.6
0.15	13.9	13.8	282.0
0.22	16.2	16.1	12.6
0.32	9.60	9.60	9.63
0.46	6.81	6.82	7.94
0.68	6.40	6.41	6.96
1.00	6.64	6.64	6.71
1.47	7.21	7.22	7.11
2.15	8.25	8.26	8.24
3.16	10.5	10.5	10.3
4.64	14.3	14.2	13.3
6.81	18.4	18.4	17.6
10.0	23.1	22.7	22.2
14.7	30.1	27.9	26.7
21.5	57.8	36.3	35.2
31.6	171.6	53.6	48.1
46.4	169.4	74.6	85.0
68.1	256.1	162.9	158.5
100.	242.6	241.4	467.7

[a] Pinatubo aerosols included.
[b] Pinatubo aerosols not included.

Table 8. Zonal Mean Data Contained in Climatology

Solar Heating	Radiative Cooling (0-3000 cm^{-1})	Additional Data
Ozone Hartley band	Ozone (rotational, ν_1, ν_2, ν_3)	Net radiative heating
Ozone Huggins band	Water vapor (rotational, ν_2)	Infrared aerosol cooling (400-3000 cm^{-1})
Ozone Chappuis band	Carbon dioxide (ν_2, ν_3)	Mean vertical velocity (w^*) in cm/s
Oxygen total ultraviolet	Total infrared cooling (sum of all the above)	Mean meridional velocity (v^*) in m/s
Oxygen near infrared (0.762, 0.688, and 1.27 μm)		Radiative relaxation times
Carbon dioxide near infrared		Global-mean radiative relaxation times
Total solar heating (sum of all the above)		Global-mean radiation balance

68.1, 46,4, and 31.6 hPa, respectively. *Gille and Lyjak* [1986] also calculated globally averaged relaxation times using LIMS data. Their results are generally consistent with ours below 1 hPa, based on comparing our figure with theirs. The differences in the mesosphere are likely due to differences in the way the LIMS data were extended in latitude and in height (for example, compare section 2 with the input data description by *Gille and Lyjak* [1986]).

4. Summary and Conclusion

In this paper we evaluated the radiative budget of the stratosphere through a detailed examination of the individual heating and cooling processes. We have carried out calculations of stratospheric radiative and dynamical parameters using 18 months of temperature and minor constituent data provided by measurements from orbiting satellites. Typically, data for 5 months common to LIMS and UARS are displayed above. Consideration of space prevents presentation of the entire 18 month climatology. However, the data, as presented above, are representative of the quality of the entire data set. We have purposely restricted our calculations to those times when the necessary satellite-derived temperature, ozone, water vapor, and nitrogen dioxide measurements are simultaneously available for the calculations.

From the calculations presented in both parts 1 and 2 we reached a number of conclusions. First, we showed that in general, the stratosphere is in radiative equilibrium on monthly timescales to within the accuracy of the satellite data, the radiative transfer algorithms, and the molecular spectroscopy databases. This result demonstrates the utility of satellite data for use in diagnosing dynamical properties. There is also a balance between the total amount of solar radiation absorbed and infrared energy emitted by the stratosphere. Second, it is necessary to include overlap between the ν_2 band of ozone and the ν_2 bands of CO_2 in the vicinity of 14 μm. This has an important impact on the radiative balance of the middle stratosphere. Third, the presence of Pinatubo aerosols increases the radiative relaxation time in the lower stratosphere. Finally, the EGA method of radiative transfer is robust for computing atmospheric radiative cooling rates.

We chose to compare results from the LIMS and UARS experiments because these are the only two extant data sets from which the diabatic heating terms can be evaluated using only the satellite-derived temperature and constituent fields. We used these fields to evaluate the diabatic circulation and found strong similarity between the diagnosed vertical velocity w^* patterns for the LIMS and UARS data despite some 13-14 years time difference. There were also similarities in the patterns of v^* diagnosed from the two data sets but with more noticeable differences in magnitude which we attribute to the natural variability of the stratosphere.

The 18 months of data described above are available for access by the community via a World Wide Web interface at url http://heat-budget.gats-inc.com. The specific parameters available in the climatology are listed in Table 8. It is intended that users can access all or part of this climatology for studies of stratospheric radiative properties or perhaps to run model calculations using the fields of heating and cooling.

Acknowledgments. We gratefully acknowledge support for this work under the Guest Investigator Program of the NASA Upper Atmosphere Research Satellite project. Thanks to Don Johnson of the University of Wisconsin for helpful advice, to Yunfei Wang of GATS, Inc., for running simulations and preparing figures, and to Tom Marshall of GATS, Inc., for assistance with the LINEPAK and EGA radiation models. Thanks also to Ellis Remsberg of NASA Langley and to Susan Solomon of NOAA Aeronomy Laboratory who provided helpful comments on the manuscripts.

References

Andrews, D. G., and M. E. McIntyre, Planetary waves in horizontal and vertical shear: The generalized Eliassen-Palm relation and the mean zonal acceleration, *J. Atmos. Sci., 33,* 2031-2048, 1976.

Barath, F. T., et al., The Upper Atmosphere Research Satellite Microwave Limb Sounder instrument, *J. Geophys. Res., 98,* 10,751-10,762, 1993.

Boyd, J., The noninteraction of waves with the zonally-averaged flow on a spherical earth and the interrelationships of eddy fluxes of energy, heat and momentum, *J. Atmos. Sci., 33*, 2285-2291, 1976.

Charney, J. G., and P. G. Drazin, Propagation of planetary scale disturbances from the lower into the upper atmosphere, *J. Geophys. Res., 66*, 83-109, 1961.

Craig, R. A., and G. Ohring, The temperature dependence of ozone radiational heating rates in the vicinity of the mesopeak, *J. Meteorol., 15*, 59-62, 1958.

Cunnold, D. M., H. Wang, W. P. Chu, and L. Froidevaux, Comparisons between Stratospheric Aerosol and Gas Experiment II and Microwave Limb Sounder ozone measurements and aliasing of SAGE II ozone trends in the lower stratosphere, *J. Geophys. Res., 101,* 10,061-10,075, 1996a.

Cunnold, D. M., L. Froidevaux, J. M. Russell, B. Connor, and A. Roche, Overview of UARS ozone validation based primarily on intercomparisons among UARS and Stratospheric Aerosol and Gas Experiment II measurements, *J. Geophys. Res., 101,* 10,335-10,350, 1996b.

Dunkerton, T., On the mean meridional mass motions of the stratosphere and mesosphere, *J. Atmos. Sci., 35*, 2325-2333, 1978.

Eluszkiewicz, J., et al., Residual circulations in the stratosphere and lower mesosphere as diagnosed from Microwave Limb Sounder data, *J. Atmos. Sci., 53*, 217-240, 1996.

Eluszkiewicz, J., D. Crisp, R. G. Grainger, A. Lambert, A. E. Roche, J. B. Kumer, and J. L. Mergenthaler, Sensitivity of the residual circulation diagnosed from the UARS data to the uncertainties in the input fields and to the inclusion of aerosols, *J. Atmos. Sci., 55*, 1739-1757, 1997.

Fishbein, E. F., et al., Validation of UARS Microwave Limb Sounder temperature and pressure, *J. Geophys. Res., 101,* 9983-10,016, 1996.

Froidevaux, L., et al., Validation of Microwave Limb Sounder ozone measurements, *J. Geophys. Res., 101,* 10,017-10,060, 1996.

Garcia, R. R., and S. Solomon, A new numerical model of the middle atmosphere, 2, Ozone and related species, *J. Geophys. Res., 99*, 12,937-12,951, 1994.

Garcia, R. R., F. Stordal, S. Solomon, and J. Kiehl, A new numerical model of the middle atmosphere, 1, Dynamical and transport of tropospheric source gases, *J. Geophys. Res., 97*, 12,967-12,991,1992.

Ghazi, A., V. Ramanathan, and R. E. Dickinson, Acceleration of Upper Stratospheric Radiative Damping: Observational Evidence, *Geophys. Res. Lett., 6*, 437-440, 1979.

Gille, J. C., and L. V. Lyjak, Radiative heating and cooling rates in the middle atmosphere, *J. Atmos. Sci., 43*, 2215-2229, 1986.

Gille, J. C., and L. V. Lyjak, The global residual mean circulation in the middle atmosphere for the northern winter period, *J. Atmos. Sci., 44*, 1437-1453, 1987.

Gille, J. C., and J. M. Russell III, The limb infrared monitor of the stratosphere: Experiment description, performance, and results, *J. Geophys. Res., 89,* 5125-5140, 1984.

Gille, J. C., J. M. Russell III, P. L. Bailey, L. L. Gordley, E. E. Remsberg, J. H. Lienesch, W. G. Planet, F. B. House, L. V. Lyjak, and S. A. Beck, Validation of temperature retrievals obtained by the limb infrared monitor of the stratosphere (LIMS) experiment on Nimbus 7, *J. Geophys. Res., 89,* 5147-5160, 1984.

Gordley, L. L., B. T. Marshall, and D. A. Chu, LINEPAK: Algorithms for modeling spectral transmittance and radiance, *J. Quant. Spectrosc. Radiat. Transfer, 52*, 563-580, 1994.

Hervig, M. E., J. M. Russell, L. L. Gordley, J. H. Park, S. R. Drayson, and T. Deshler, Validation of aerosol measurements from the Halogen Occultation Experiment, *J. Geophys. Res., 101*, 10,267-10,275, 1996.

Kellog, W. W., Chemical heating above the polar mesopause in winter, *J. Meteorol., 18*, 373-381, 1961.

Kiehl, J. T., and S. Solomon, On the radiative balance of the stratosphere, *J. Atmos. Sci., 43*, 1525-1534, 1986.

Lahoz, W. A., et al., Validation of UARS Microwave Limb Sounder 183 GHz H_2O measurements, *J. Geophys. Res., 101,* 10,129-10,149, 1996.

London, J., Radiative energy sources and sinks in the stratosphere and mesosphere, in *Proceedings of the NATO Advanced Study Institute on Atmospheric Ozone*, edited by A. C. Aiken, 703-721, *Rep. FAA-EE-80-20*, U.S. Dep. of Transp., Washington, D. C., 1980.

Marshall, B. T., L. L. Gordley, and D. A. Chu, BANDPAK: Algorithms for modeling broadband transmission and radiance, *J. Quant. Spectrosc. Radiat. Transfer, 52*, 581-599, 1994.

Mertens, C. J., M. G. Mlynczak, R. R. Garcia, and R. Portmann, A detailed evaluation of the stratospheric heat budget, 1, Radiation transfer, *J. Geophys. Res.,* this issue.

Mlynczak, M. G., and S. R. Drayson, Calculation of infrared limb emission by ozone in the terrestrial middle atmosphere, 1, Source functions, *J. Geophys. Res., 95*, 16,497-16,511, 1990a.

Mlynczak, M. G., and S. R. Drayson, Calculation of infrared limb emission by ozone in the terrestrial midddle atmosphere, 2, Emission calculations, *J. Geophys. Res., 95*, 16,512-16,521, 1990b.

Murgatroyd, R. J., and R. M. Goody, Sources and sinks of radiative energy from 30 to 90 km, *Q. J. R. Meteorol. Soc., 84*, 225-234, 1958.

Murgatroyd, R. J., and F. Singleton, Possible meridional circulations in the stratosphere and mesosphere, *Q. J. R. Meteorol. Soc., 87*, 225-234, 1961.

Olaguer, E. P., H. Yang, and K. K. Tung, A Reexamination of the radiative balance of the stratosphere, *J. Atmos. Sci., 49*, 1242-1261, 1992.

Pawson, S., and R. S. Harwood, Monthly-mean diabatic circulations in the stratosphere, *Q. J. R. Meteorol. Soc., 115*, 807-840, 1989.

Pawson, S., R. S. Harwood, and J. D. Haigh, A study of the radiative dissipation of planetary waves using satellite data, *J. Atmos. Sci., 49*, 1304-1317, 1992.

Ramanathan, V., Radiative transfer within the Earth's troposphere and stratosphere: A simplified radiative-convective model, *J. Atmos. Sci., 33*, 1330-1346, 1976.

Ramanathan, V., B. R. Barkstrom, and E. F. Harrison, Climate and the Earth's radiation budget, *Physics Today, 42*, 22-32, 1989.

Reber, C. A., C. E. Trevathan, R. J. McNeal, and M. R. Luther, The Upper Atmosphere Research Satellite (UARS) mission, *J. Geophys. Res., 98*, 10,643-10,647, 1993.

Reburn, W. J., J. J. Remedios, P. E. Morris, C. D. Rogers, F. W. Taylor, B. J. Kerridge, R. J. Knight, J. Ballard, J. B. Kumer, and S. T. Massie, Validation of nitrogen dioxide measurements from the improved stratospheric and mesospheric sounder, *J. Geophys. Res., 101,* 9873-9895, 1996.

Remsberg, E. E., J. M. Russell III, J. C. Gille, L. L. Gordley, P. L. Bailey, W. G. Planet, and J. E. Harries, The Validation of Nimbus 7 LIMS measurements of ozone, *J. Geophys. Res., 89*, 5161-5178, 1984.

Remsberg, E. E., K. V. Haggard, and J. M. Russell III, Estimation of synoptic fields of middle atmosphere parameters from Nimbus-7 LIMS profile data, *J. Atmos. Ocean. Technol., 7*, 689-705, 1990.

Remsberg, E. E., P. P. Bhatt, and T. Miles, An assessment of satellite temperature distributions used to derive the net diabatic transport for zonally averaged models of the middle atmosphere, *J. Geophys. Res., 99*, 23,001-23,018, 1994.

Roche, A. E., J. B. Kumer, J. L. Mergenthaler, G. A. Ely, W. G. Uplinger, J. F. Potter, T. C. James, and L. W. Sterritt, The cryogenic limb array etalon spectrometer (CLAES) on UARS: Experiment description and performance, *J. Geophys. Res., 98*, 10,763-10,775, 1993.

Russell, J. M., III, J. C. Gille, E. E. Remsberg, L. L. Gordley, P. L. Bailey, S. R. Drayson, H. Fischer, A. Girard, J. E. Harries, and W. F. J. Evans, Validation of nitrogen dioxide results measured by the limb infrared monitor of the stratosphere (LIMS) experiment on Nimbus 7, *J. Geophys. Res., 89*, 5009-5107, 1984a.

Russell, J. M., III, J. C. Gille, E. E. Remsberg, L. L. Gordley, P. L. Bailey, H. Fischer, A. Girard, S. R. Drayson, W. F. J. Evans, and J. E. Harries, Validation of water vapor results measured by the limb infrared monitor of the stratosphere experiment on Nimbus 7, *J. Geophys. Res., 89*, 5115-5124, 1984b.

Russell, J. M., III, L. L. Gordley, J. H. Park, S. R. Drayson, W. D. Hesketh, R. J. Cicerone, A. F. Tuck, J. E. Frederick, J. E. Harries, and P. J. Crutzen, The Halogen Occultation Experiment, *J. Geophys. Res., 98*, 10,777-10,797, 1993.

Solomon, S., J. T. Kiehl, R. R. Garcia, and W. Grose, Tracer transport by the diabatic circulation deduced from satellite observations, *J. Atmos. Sci., 43*, 1603-1617, 1986a.

Solomon, S., J. T. Kiehl, B. J. Kerridge, E. E. Remsberg, and J. M. Russell III, Evidence for nonlocal thermodynamic equilibrium in the ν_3 mode of mesospheric ozone, *J. Geophys. Res., 91*, 9865-9876, 1986b.

Taylor, F. W., et al., Remote sensing of atmospheric structure and composition by pressure modulator radiometry from space: The ISAMS experiment on UARS, *J. Geophys. Res., 98*, 10,799-10,814, 1993.

VonderHaar, T. H., and V. E. Suomi, Measurements of the Earth's radiation budget from satellites during a five-year period, 1, Extended time and space means, *J. Atmos. Sci. 28*, 305-314, 1971.

Waters, J. W., L. Froidevaux, W. G. Read, G. L. Manney, L. S. Elson, D. A. Flower, R. F., Jarnot, and R. S. Harwood, Stratospheric ClO and ozone from the Microwave Limb Sounder on the Upper Atmosphere Research Satellite, *Nature, 362*, 597-602, 1993.

Young, C., and E. E. Epstein, Atomic oxygen in the polar winter mesosphere, *J. Atmos. Sci., 19*, 435-443, 1962.

R. R. Garcia, National Center for Atmospheric Research, P.O. Box 3000, Boulder, CO 80303. (rgarcia@garcia.acd.ucar.edu)

C. J. Mertens, GATS, Inc., 11864 Canon Blvd., Suite 101, Newport News, VA 23606. (c.j.mertens@gats-inc.com)

M. G. Mlynczak, NASA Langley Research Center, Mail Stop 401B, Hampton, VA 23681-0001. (m.g.mlynczak@larc.nasa.gov)

R. W. Portmann, NOAA Aeronomy Laboratory, 325 Broadway, Mail Code R/E/AL 8, Boulder, CO 80303. (bportmann@al.noaa.gov)

(Received May 8, 1998; revised September 14, 1998; accepted November 17, 1998.)